Fracture & Fatigue Analyses: SGBEM-FEM or XFEM? Part 1: 2D Structures

Leiting Dong[1,2]**, Satya N. Atluri**[1,3]

Abstract: In this paper, and its companion Part 2 [Dong and Atluri (2013b)], the Symmetric Galerkin Boundary Element Method (SGBEM), and the SGBEM-FEM alternating/coupling methods, are compared with the recently popularized Extended Finite Element Method (XFEM), for analyzing fracture and fatigue crack propagation in complex structural geometries. The historical development, and the theoretical/algorithmic formulations, of each method are succinctly reviewed. The advantages and disadvantages of each method are critically discussed. A comprehensive evaluation of the performances of the SGBEM-based methods, and their comparison with XFEM, in modeling cracked solid structures undergoing fatigue crack-growth is carried out. A thorough examination of a large set of numerical examples of varying degrees of complexity shows that, the SGBEM-based methods: (a) are far more accurate than XFEM for computing stress intensity factors, and thus the fatigue-crack-growth-rates; (b) require significantly coarser and lower-quality meshes than in XFEM, and thus result in significant savings of computational costs, and more importantly in considerable savings of the human-labor-costs of generating meshes; (c) require minimal effort for modeling the non-collinear/non-planar propagation of cracks under fatigue, without using the Level Set or Fast Marching methods to track the crack surface; (d) can easily perform fracture and fatigue analysis of complex structures, such as repaired cracked structures with composite patches, and damage in heterogeneous materials. It is thus concluded that the SGBEM-based methods, and alternating methods, which were developed over the past 20-30 years by Atluri and his many collaborators, are by far the best methods for analyzing fracture and non-planar fatigue crack propagation in complex structures, and are thus valuable for inclusion in general-purpose, off-the-shelf commercial software for structural analyses. This objective is pursued by the authors.

[1] Center for Aerospace Research & Education, University of California, Irvine
[2] Department of Engineering Mechanics, Hohai University
[3] Distinguished Adjunct-Professor of Multi-Disciplinary Engineering and Computer Science, King Abdulaziz University, Saudi Arabia

1 Introduction

Modeling the fracture and fatigue behavior of cracked solid structures is an important task in the structural integrity assessment and damage tolerance analyses of civil, mechanical, aerospace, and military structures, see the comprehensive Monograph [Atluri (1998)]. In spite of its wide-spread popularity, the traditional finite element method, with simple polynomial interpolations, is unsuitable for modeling cracks and their propagation, partially due to the high-inefficiency of approximating stress & strain-singularities using polynomial FEM shape functions. In order to overcome this difficulty, embedded-singularity elements by [Tong, Pian and Lasry (1973); Atluri, Kobayashi and Nakagaki (1975)], and singular quarter-point elements by [Henshell and Shaw (1975) and Barsoum (1976)], among others, were developed in the 1970s, in order to capture the crack-tip/ crack-front singular field. Many such related developments were summarized in the Monograph [Atluri (1986)], and they are now widely available in many commercial FEM software, such as ANSYS and ABAQUS. However, the need for constant remeshing makes the automatic fatigue-crack-propagation analyses with FEM extremely difficult, if not impossible.

The later method of the so-called XFEM (Extended Finite element Method), which was put forward first in [Moës, Dolbow and Belytschko (1999)], became wildly popular in the past decade. It is interesting to note that, according to ISI's webofknowledge, the paper by [Moës, Dolbow, and Belytschko (1999)] has so far (January 2013) already been cited in literature, 1140 times!. Also, a quick search of "XFEM" on Google Scholar returns more than 3500 results for papers published so far on the subject of XFEM. Considering the average research cost in writing an archival research paper (a very modest estimate of about 50,000 US $ per paper), it can be quickly seen that about 200 Million US $s have so far been spent in developing the XFEM. Two special issues (*Int. J. Numer. Meth. Engng., vol. 86, issues 4-5,2011),* have been devoted to the development and application of XFEM. Three major international conferences (*XFEM 2009, XFEM 2011, XFEM 2013*), in the past few years have been entirely devoted to the discussions of XFEM. However, XFEM differs very little in theory from the embedded-singularity elements developed in the 1970s and cited above. Both the widely popular XFEM of the past decade, and the embedded-singularity elements of the 1970s, use crack-tip singular fields to enrich the trial functions. Both of them use variational principles or symmetric Galerkin weak-forms to develop FEM equations. And both of them use path-independent/ domain-independent integrals as in [Rice (1968);

Atluri (1982); Nishioka and Atluri (1983); Nikishkov and Atluri (1987a,b)], or their interaction-integral variants [Chen and Shield (1977)], among other techniques, to extract and to evaluate the stress intensity factors from the computed displacement/strain/stress solutions. Moreover, for both the XFEM and the much-earlier embedded-singularity elements, singular enrichment is confined only to the elements which are immediately adjacent to the crack-tip/ crack-front. Therefore, as seen in most XFEM publications in the open literature, an extremely fine and good-quality mesh is still necessary to capture the high gradients of the stress field, at locations near to the crack tips/ crack fronts.

In a fundamentally different mathematical way, after the derivation of analytical solution for embedded elliptical cracks whose faces are subjected to arbitrary normal and shear tractions, the first paper on a highly-accurate Finite Element (Schwartz-Neumann) Alternating Method (FEAM) was published in [Nishioka and Atluri (1983)]. The FEAM uses the Schwartz-Neumann alternation between a crude and simple finite element solution for an uncracked structure, and the analytical solution for an infinite body containing the crack. The success of this method is mostly due to the work of [Vijayakumar and Atluri (1981)], in which the analytical solutions for an embedded elliptical crack, the faces of which are subjected to arbitrary normal and shear tractions, are derived, and they are now popularly named as the VNA solutions. Subsequent 3D and 2D variants of the finite element alternating methods were successfully developed and applied to perform structural integrity and damage tolerance analysis of many practical engineering structures, including: cracked stiffened panels with/without composite-patch repairs in [Park, Ogiso, and Atluri (1992)]; multi-site fatigue damage of aging aircraft structural elements in [Park, Singh, Pyo, and Atluri (1995)]; elastic-plastic wide-spread fatigue damage in ductile panels [Pyo, Okada and Atluri (1995)]; fatigue growth of cracks in 3D aircraft components in [O'Donoghue, Atluri, and Pipkins (1995)]; cracks emanating from fastener holes in [Park and Atluri (1998)] and many many others in the literature. Very recently, the SGBEM-FEM Alternating method (involving the alternation between the very crude FEM solution of the uncracked structure, and an SGBEM solution for a small region enveloping the arbitrary non-planar 3-D crack, was developed for arbitrary three-dimensional non-planar growth of embedded as well as surface cracks in [Nikishkov, Park and Atluri (2001), Han and Atluri (2002)]. Most recently, in [Dong and Aluri (2012,2013a)], a SGBEM super element[1] was developed for direct coupling of SGBEM and FEM, for fracture and fatigue analysis of complex 2D solid structures and materials. The motivation for this series of works, by Atluri and many of his collaborators since the 1980s, is

---

[1] SGBEM Super Element is named as SGBEM Voronoi Cell (SVC), when it is used to model heterogenous materials, in [Dong and Atluri(2013a)]

to explore the advantageous features of each computational method: model complicated uncracked structures with simple FEMs, and model crack-singularities by mathematical methods such as complex variables, special functions, BIEs, and by SGBEMs.

In order to find the simplest and the best method, among the many cited above, for modeling fracture and fatigue-crack-propagation in solid structures, many numerical examples are computed in the present study. The performance of SGBEM-based methods is compared to with that of XFEM. Various highly-cited papers on crack analysis by XFEM are first chosen. The same examples as presented in these highly cited XFEM papers are solved by the SGBEM-based methods developed by the authors. The numerical examples for two-dimensional problems are shown in this paper, and those for three-dimensional problems are presented in a companion Part 2. Numerical results show that the SGBEM and the SGBEM-FEM alternating/coupling method are far more accurate than the XFEM in computing stress intensity factors. SGBEM-related methods require very coarse meshes and very little computational cost, while XFEM requires very fine meshes and involve very high computational burdens. Analyses of fatigue-crack-propagation by SGBEM requires a minimal effort, by simply adding an element to each crack tip, but special methods such as Level Sets and Fast Marching Methods are necessary for XFEM, to track the growing surfaces of the cracks. Several examples of cracked structures which are repaired with composite patches, and damaged heterogeneous materials, also demonstrate the power of SGBEM-based methods for modeling complex structures with stationary or propagating cracks.

The rest of this paper is organized as follows: in section 2, we review the formulation of XFEM; in section 3, we review SGBEM and its coupling with FEM; in section 4, we compare these two methods in many numerical examples of two-dimensional problems; in section 5, we complete this paper with some concluding remarks.

2   XFEM: Theory and Algorithmic Formulations

Consider a linear elastic solid Ω undergoing an infinitesimal elasto-static deformation, where body forces can be neglected. $\sigma_{ij}, \varepsilon_{ij}, u_i$ are Cartesian components of the stress tensor, strain tensor and displacement vector respectively. $\bar{u}_i, \bar{t}_i$ are Cartesian components of the prescribed displacement at S_u and traction at S_t. We use $(\quad)_{,i}$ to denote differentiation with respect to x_i. The governing differential equations can be expressed in terms of displacements, which are the Navier's equations:

$$\left(E_{ijkl} u_{k,l} \right)_{,i} = 0 \qquad \text{in } \Omega \tag{1}$$

For isotropic plane elasticity,

$$E_{ijkl} = \mu \left(\tfrac{2\bar{v}}{1-2\bar{v}} \delta_{ij}\delta_{kl} + \delta_{ik}\delta_{jl} + \delta_{il}\delta_{jk} \right) \qquad i,j,k,l = 1,2$$

$$\bar{v} = \begin{cases} v \text{ for plane strain problems} \\ \frac{v}{1+v} \text{ for plane stress problems} \end{cases} \tag{2}$$

For 3D isotropic elasticity

$$E_{ijkl} = \mu \left(\frac{2v}{1-2v} \delta_{ij}\delta_{kl} + \delta_{ik}\delta_{jl} + \delta_{il}\delta_{jk} \right) \qquad i,j,k,l = 1,2,3 \tag{3}$$

Boundary conditions are:

$$u_i = \bar{u}_i \text{ at } S_u \tag{4}$$

$$t_i = \bar{t}_i \text{ at } S_t \tag{5}$$

Similar to traditional finite elements, XFEM equations can be developed using the single-field variational principle, see [Atluri (2005)], which corresponds to the stationarity of the following scalar functional, which is a function of the trial displacement field u_k that is continuous and satisfies (4) a-priori:

$$\pi(u_k) = \int_\Omega \frac{1}{2} E_{ijkl} u_{i,j} u_{k,l} d\Omega - \int_{S_t} \bar{t}_i u_i dS \tag{6}$$

Traditional FEM uses polynomial shape functions $\phi^{(i)}$ to construct the trial displacement field:

$$u_k = \sum_{i \in I} u_k^{(i)} \phi^{(i)} \tag{7}$$

For a cracked solid as shown in Fig.1, XFEM introduces two additional fields to model the displacement discontinuity across crack surface and the stress singularity at crack-tips/ crack-fronts:

$$u_k = \sum_{i \in I} u_k^{(i)} \phi^{(i)} + \sum_{i \in J} a_k^{(i)} \phi^{(i)} H + \sum_{i \in K} \sum_j b_{kj}^{(i)} \phi^{(i)} F_j \tag{8}$$

I is the set of all nodes. J is the set of the nodes which are immediately adjacent to the crack surface. K is the set of the nodes which are immediately adjacent to the crack tips or crack fronts. H is a spatial Heaviside function, which equals to 1 at one side of the crack, and 0 at the other side of the crack. F_j is the singularity enrichment for elements directly adjacent to crack-tips or crack-fronts. For

both two-dimensional and three-dimensional problems, F_j is a function of local polar coordinates, see [Moës, Dolbow and Belytschko (1999), Moës, Gravouil and Belytschko (2002)]:

$$F_1 = \sqrt{r}\sin\left(\frac{\theta}{2}\right), F_2 = \sqrt{r}\cos\left(\frac{\theta}{2}\right),$$

$$F_3 = \sqrt{r}\sin\left(\frac{\theta}{2}\right)\sin(\theta), F_4 = \sqrt{r}\cos\left(\frac{\theta}{2}\right)\sin(\theta) \tag{9}$$
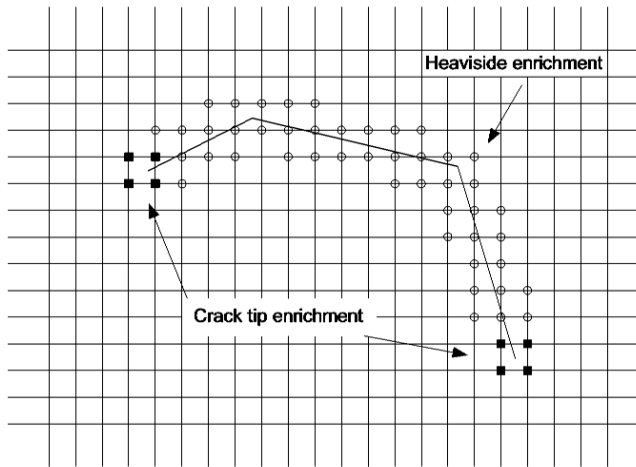
Figure 1: Enrichments for XFEM

Substituting the trial displacement fields (8) into (6), stationarity conditions lead to a system of equations similar to those for traditional FEM:

$$\begin{bmatrix} k_{uu} & k_{ua} & k_{ub} \\ k_{au} & k_{aa} & k_{ab} \\ k_{bu} & k_{ba} & k_{bb} \end{bmatrix} \begin{Bmatrix} u \\ a \\ b \end{Bmatrix} = \begin{Bmatrix} f_u \\ f_a \\ f_b \end{Bmatrix} \tag{10}$$

u, a, b represent the nodal displacements, Heaviside enrichments, and crack-tip/ crack-front singular enrichments respectively. Once they are solved, spatial displacements and stresses can be computed. The stress-intensity factors can be computed using path-independent or domain independent integrals, or their variants in an interaction integral form, as in [Eshelby (1951); Rice (1968); Atluri (1982); Nishioka and Atluri (1983); Nikishkov and Atluri (1987a,b)]. In most of the XFEM

literature, the interaction integral as in [Chen and Shield (1977); Atluri (1998)] is used to compute the stress intensity factors:

$$I(u_i, \tilde{u}_i^{(k)}) = J(u_i + \tilde{u}_i^{(k)}) - J(u_i) - J(\tilde{u}_i^{(k)})$$

$$= \int\limits_C \left[\sigma_{ij} \tilde{\varepsilon}_{ij}^{(k)} n_1 - n_j \tilde{\sigma}_{ij} \frac{\partial \tilde{u}_i^{(k)}}{\partial x_1} - n_j \tilde{\sigma}_{ij}^{(k)} \frac{\partial u_i}{\partial x_1} \right] dS \tag{11}$$

where $\tilde{u}_i^{(k)}, \tilde{\varepsilon}_{ij}^{(k)}, \tilde{\sigma}_{ij}^{(k)}$ denotes the displacements and stresses for an auxiliary pure mode k crack. Equation (11) can also be evaluated in an equivalent domain integral method, as shown in [Nikishkov and Atluri (1987a, b); Atluri (1998)].

The stress intensity factors can be determined as:

$$K_k(u_i) = \alpha \frac{I(u_i, \tilde{u}_i^{(k)})}{K_k\left(\tilde{u}_i^{(k)}\right)} \tag{12}$$

α is a constant depending on the material properties μ, ν, the mode number k, and whether it is 2D plane stress, plane strain, or 3D problems.

Fatigue growth direction of the crack-tip can be determined using maximum tangential stress or maximum strain energy criteria, see [Atluri (1998)]. Also, the crack extension distance can be computed using various fatigue laws such as Paris or Forman equations, once stress intensity factors are correctly computed. However, for XFEM, a special technique is needed to track the crack surface at each fatigue step. The most popular one in the XFEM literature is to use the Level Set function, see [Stolarska, Chopp, Moës, Belytschko (2001); Moës, Gravouil and Belytschko (2002)]. A frequently used Level-Set function for the initial crack surface is the signed-distance function:

$$\varphi(\mathbf{x}, t_0) = \pm \min \|\mathbf{x} - \mathbf{x}^*\|, \ \mathbf{x}^* \in \Gamma \tag{13}$$

Γ is the surface describing the initial crack, and $\|\|$ is the Euclidean distance. Therefore the magnitude of φ is equal to the shortest distance of the point $\mathbf{x}$ to the surface Γ. The sign of φ is different on the two opposite sides of the surface Γ. The crack surface can be described by the equation $\varphi = 0$. However, because the Level Sets have to be defined for a closed interface or an infinite interface, Γ has to be extended beyond the crack fronts. The crack front is defined by the intersection between the surface Γ and a orthogonal surface S, which is described by another Level Set function ψ, see Fig. 2.

For XFEM application, φ and ψ are stored and computed at each time step in a

discretized way, using FEM shape functions:

$$\varphi(\mathbf{x},t) = \sum_{i \in I} \phi^{(i)}(\mathbf{x}) \varphi(\mathbf{x}^{(i)},t)$$
$$\psi(\mathbf{x},t) = \sum_{i \in I} \phi^{(i)}(\mathbf{x}) \psi(\mathbf{x}^{(i)},t)$$

(14)

In order to have a relatively accurate approximation of the Level Set functions, a fine mesh is again necessary. Computing the Level Set function over the domain is time-consuming in itself. In addition, the updating of the Level Set function in each fatigue step adds much more of a computational burden. Methods such as Fast-Marching-Method have been used to compute and update the Level Set function in each time step, see [Sukumar, Chopp, and Moran (2002), Sukumar, Chopp, Béchet, and Moës (2008)] for details.
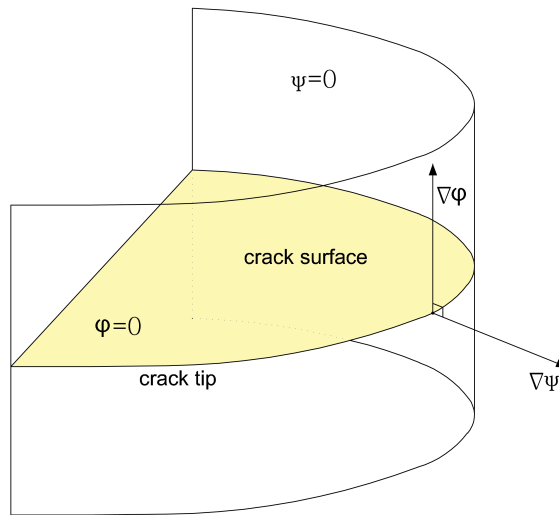
Figure 2: The two Level Sets defining the crack surface and the crack-front

3   SGBEM and SGBEM Alternating/Coupling Method: Theory and Formulation

The Symmetric Galerkin Boundary Element Method (SGBEM) has several advantages over collocation/direct and dual BEMs [Rizzo (1967), Hong and Chen (1988)], such as resulting in a symmetrical coefficient matrix of the system of

equations, and the avoidance of the need to treat sharp corners specially, etc. Early derivations of SGBEMs involve regularization of hyper-singular integrals, as in [Frangi and Novati (1996); Bonnet, Maier and Polizzotto (1998); Li, Mear and Xiao (1998); Frangi, Novati, Springhetti, Rovizzi (2002)]. A systematic procedure to develop weakly-singular symmetric Galerkin boundary integral equations was presented by [Han and Atluri (2003,2007)]. The derivation of the this simple formulation involves only the non-hyper singular integral equations for tractions, based on the original work reported in [Okada, Rajiyah and Atluri (1988,1989)]. It was used to analyze cracked 3D solids with surface flaws in [Han and Atluri (2002)], and cracked 2D structures and heterogeneous materials in [Dong and Atluri (2012,2013a)].

For a domain of interest as in Fig. 3, with source point **x** and target point ξ, 3D weakly-singular symmetric Galerkin BIEs for displacements and tractions are developed in [Han and Atluri(2003)].
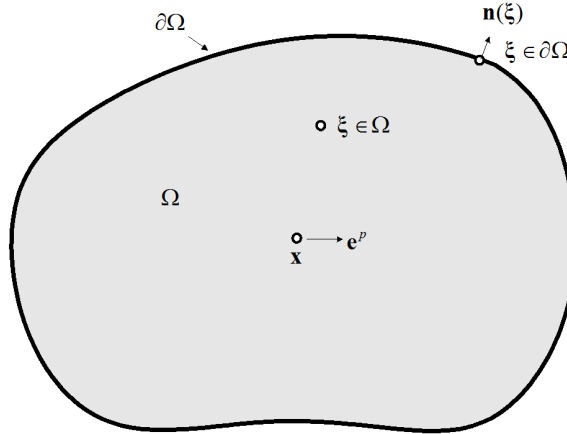
Figure 3: A solution domain with source point **x** and target point ξ, taken from [Han and Atluri (2002)]

The displacement BIE is:

$$\frac{1}{2} \int_{\partial\Omega} v_p(\mathbf{x}) u_p(\mathbf{x}) dS_x$$

$$= \int_{\partial\Omega} v_p(\mathbf{x}) dS_x \int_{\partial\Omega} t_j(\xi) u_j^{*p}(\mathbf{x},\xi) dS_\xi$$

$$+ \int_{\partial\Omega} v_p(\mathbf{x}) dS_x \int_{\partial\Omega} D_i(\xi) u_j(\xi) G_{ij}^{*p}(\mathbf{x},\xi) dS_\xi \qquad (15)$$

$$+ \int_{\partial\Omega} v_p(\mathbf{x}) dS_x \int_{\partial\Omega} n_i(\xi) u_j(\xi) \phi_{ij}^{*p}(\mathbf{x},\xi) dS_\xi$$

And the corresponding traction BIE is:

$$-\frac{1}{2}\int_{\partial\Omega} w_b(\mathbf{x}) t_b(\mathbf{x}) dS_{\mathbf{x}}$$

$$= \int_{\partial\Omega} D_a(\mathbf{x}) w_b(\mathbf{x}) dS_{\mathbf{x}} \int_{\partial\Omega} t_q(\boldsymbol{\xi}) G_{ab}^{*q}(\mathbf{x},\boldsymbol{\xi}) dS_{\boldsymbol{\xi}}$$

$$- \int_{\partial\Omega} w_b(\mathbf{x}) dS_{\mathbf{x}} \int_{\partial\Omega} n_a(\mathbf{x}) t_q(\boldsymbol{\xi}) \phi_{ab}^{*q}(\mathbf{x},\boldsymbol{\xi}) dS_{\boldsymbol{\xi}}$$

$$+ \int_{\partial\Omega} D_a(\mathbf{x}) w_b(\mathbf{x}) dS_{\mathbf{x}} \int_{\partial\Omega} D_p(\boldsymbol{\xi}) u_q(\boldsymbol{\xi}) H_{abpq}^*(\mathbf{x},\boldsymbol{\xi}) dS_{\boldsymbol{\xi}}$$

(16)

In equation (15) and (16), D_a is a surface tangential operator:

$$D_a(\boldsymbol{\xi}) = n_r(\boldsymbol{\xi}) e_{rsa} \frac{\partial}{\partial \xi_s}$$

$$D_a(\mathbf{x}) = n_r(\mathbf{x}) e_{rsa} \frac{\partial}{\partial x_s}$$

(17)
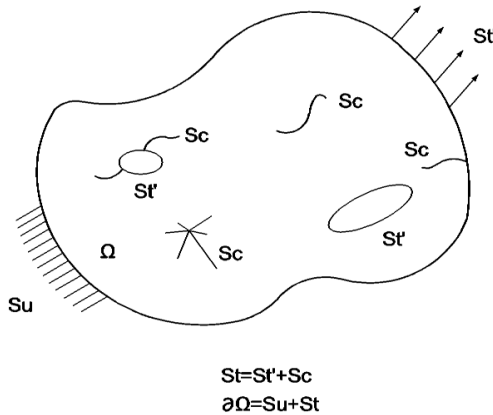
Figure 4: A defective solid with arbitrary cavities and cracks

Kernels functions $u_j^{*p}, G_{ab}^{*q}, \phi_{ab}^{*q}, H_{abpq}^*$ can be found in [Han and Atluri (2003)], which are all weakly-singular, making the implementation of the current BIEs very simple.

By applying the displacement BIE (15) to S_u, where displacements are prescribed, and applying the traction BIE (16) to $S_{t'}$, where tractions are prescribed, and applying the traction BIE (16) to S_c, which is the crack surface, a symmetric system of

equations can be obtained.

$$
\begin{bmatrix}
\mathbf{A_{pp}} & \mathbf{A_{pq}} & \mathbf{A_{pr}} \\
\mathbf{A_{qp}} & \mathbf{A_{qq}} & \mathbf{A_{qr}} \\
\mathbf{A_{rp}} & \mathbf{A_{rq}} & \mathbf{A_{rr}}
\end{bmatrix}
\begin{Bmatrix} \mathbf{p} \\ \mathbf{q} \\ \mathbf{r} \end{Bmatrix}
=
\begin{Bmatrix} \mathbf{f_p} \\ \mathbf{f_q} \\ \mathbf{f_r} \end{Bmatrix}
\tag{18}
$$

where $\mathbf{p}, \mathbf{q}, \mathbf{r}$ denotes the unknown tractions at S_u, unknown displacements at $S_{t'}$, and unknown displacement discontinuities at S_c respectively.

With the displacements and tractions being first determined at the boundary and crack surface, the displacements, strains and stress at any point in the domain can be computed using the non-hyper singular BIEs of [Okada, Rajiyah and Atluri (1988,1989)]. Therefore, the path-independent or domain-independent integrals can still be used to compute the stress intensity factors. However, with the singular quarter-point boundary elements at the crack face, stress intensity factors can also be directly computed using the displacement discontinuity at the crack-front elements, see [Nikishkov, Park and Atluri (2001)].

For fatigue growth of cracks, there is no-need to use any other special technique to describe the crack surface, such as the Level Sets used in XFEM. The crack surface is already efficiently described by boundary elements. In each fatigue step, a minimal effort is needed: one can simply extend the crack by adding some additional elements at the crack-tip/ crack front. This greatly saves the computational time for fatigue-crack-propagation analyses, as compared to the complicated Level Set Method, or the Fast Marching Method, and other complicated methods required in XFEM.

To further explore the advantage of both FEM and SGBEM, [Han and Atluri (2002)] coupled FEM and SGBEM indirectly, using the Schwartz-Neumann Alternating Method. As shown in Fig. 5, simple FEM is used to model the global uncracked structure, and SGBEM is used to model the local cracked subdomain. By imposing residual stresses at the global and the local boundaries in an alternating procedure, the solution of the original problem is obtained by superposing the solution of each individual sub-problem.

The great flexibility of this SGBEM-FEM alternating method is obvious. The SGBEM mesh of the cracked sub-domain is totally independent of the crude FEM mesh of the uncracked global structure. Because the SGBEM is used to capture the stress singularity at crack-tips/ crack fronts, a very coarse mesh can be used for FEM model of the uncracked global structure. Since FEM is used to model the uncracked global structure, large-scale structures can be efficiently modeled.

In order to model complicated solid structures, such as cracked stiffened panels and microcracks in heterogeneous solids, the SGBEM super element is developed in [Dong and Alturi (2012, 2013a)]. By applying the displacement BIE (15) and the
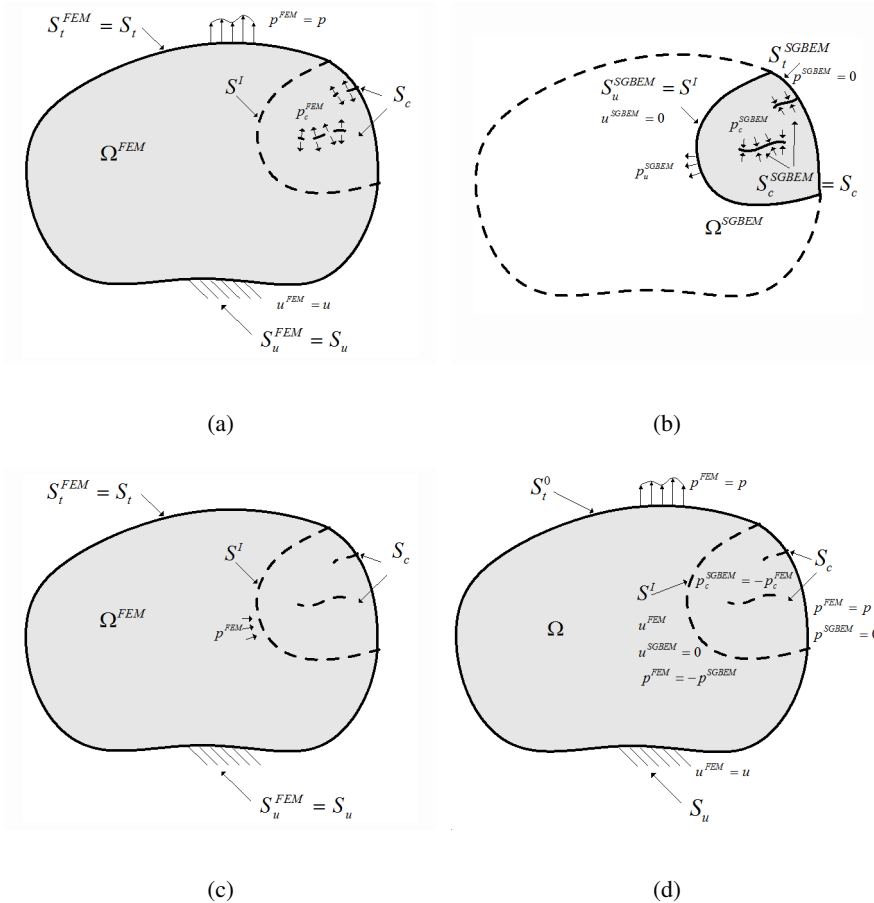
Figure 5: Superposition principle for FEM-SGBEM alternating method: (a) the uncracked body for FEM, (b) the local domain containing cracks for SGBEM, (c) FEM model subjected to residual loads, (d) alternating solution for the original problem, taken from [Han and Atluri (2002)]

traction BIE (16) to the whole boundary, and rearranging the BIEs by a few mathematical manipulations, a stiffness matrix and a force vector for the local subdomain is developed:

$$\begin{pmatrix} \delta\mathbf{q} \\ \delta\mathbf{r} \end{pmatrix}^T \begin{bmatrix} \mathbf{K_{qq}} & \mathbf{K_{qr}} \\ \mathbf{K_{rq}} & \mathbf{K_{rr}} \end{bmatrix} \begin{pmatrix} \mathbf{q} \\ \mathbf{r} \end{pmatrix} = \begin{pmatrix} \delta\mathbf{q} \\ \delta\mathbf{r} \end{pmatrix}^T \begin{pmatrix} \mathbf{Q} \\ \mathbf{R} \end{pmatrix} \qquad (19)$$

The super element can contain arbitrary voids, inclusions, and cracks. The stiff-
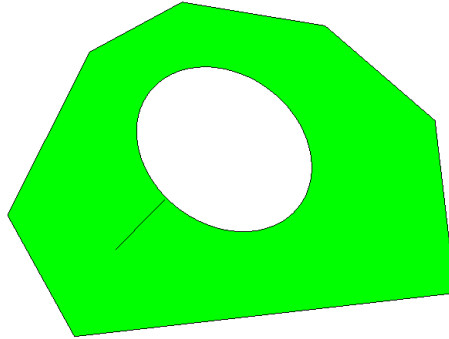
Figure 6: A SGBEM super element with arbitrary embedded inclusions/voids, and cracks.

ness matrix and the force vector have clear physical meanings, similar to those of traditional displacement FEMs, and are related to strain energy and work done. A direct coupling of the super element and FEM, and coupling of different super elements, can be achieved by the simple assembly procedure. Therefore, SGBEM super element can be easily implemented in standard commercial FEM routines. The fracture and fatigue-crack-propagation analyses of composite structures, and heterogeneous materials, also demonstrate the power of the SGBEM super elements.

4 Numerical Examples

In this section, the SGBEM and SGBEM super element- based methods are compared to the XFEM, by analyzing several examples. All the XFEM examples are chosen from the most-cited papers on XFEM in the open literature, up to the current time (2013). All the SGBEM-based results are generated by the authors, using a simple code developed by the authors (which will soon be embedded in an off-the-shelf commercial FEM software to be used for modeling un-cracked structures), on a PC with an Intel Core i5 Processor.

Example 1. An Embedded Through-Thickness Crack

First, we solve the very simple problem of an embedded through-thickness crack. A crack of length $2a$ is located at the center of a plate of $2b$ width and $2h$ height. Normal stress σ is applied on the upper and lower edges. This is shown in Fig. 7
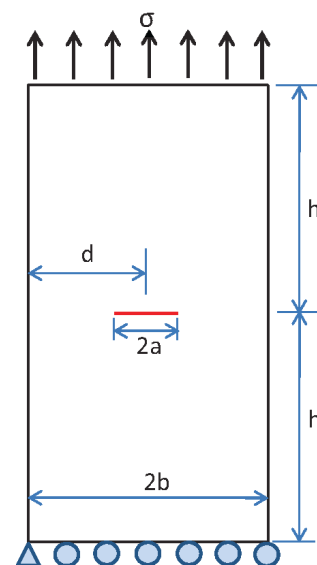
Figure 7: An Embedded Through-thickness Crack

with $a/b = 0.1$, $h/b = 1.5$. For this problem, [Tada, Paris, and Irwin (2000)] gives $\frac{K_1}{\sigma\sqrt{\pi a}} = 1.006$.

This problem was solved by XFEM in [Huang, Sukumar, and Prévost (2003)]. Two mesh configurations were used, see Fig. 8. Even though this is probably the simplest problem of fracture mechanics, when only a half of the plate is modeled considering the symmetry condition, 5000 bilinear rectangular elements are used in the structured mesh, and 3362 triangular elements are used in the unstructured mesh. The XFEM computed normalized stress intensity factor is listed in Tab. 1 for the structured mesh, and listed in Tab. 2 for the unstructured mesh. For each mesh, the stress intensity factor is computed using the domain form of the interaction integral method as discussed in section 2. The influence of domain radius r_d on the computed stress intensity factors is also shown in Tab.1 and Tab. 2. We can see that, with a strictly structured mesh, XFEM gives an accurate solution with 0.1% error, only if a large integration radius is used, (more than $0.5a$). But, as is well known, for curved cracks, using a large radius involves significant error, because the *J*-integral is no longer path-independent for curved-cracks. On the other hand, with an unstructured mesh, even with a very large radius for integration, XFEM gives a solution with an error of around 1.5%.

This problem is also solved with 2 different SGBEM meshes, see Fig. 9. In the first

case, we use only one 1 element for each side of the plate and 2 elements to mesh the crack, with a total of only 7 nodes, the least possible, for this problem!. In the second case, we use two elements to mesh each side of the plate and 4 elements to mesh the crack, with a total of only 13 nodes!. The computational results for the SGBEM-based method are shown in Tab. 3. As can be seen, extremely accurate results are obtained, even with these very coarse meshes.

Table 1: Normalized SIFs for the center crack problem (structured mesh with 5000 finite elements), Using XFEM: [Huang, Sukumar, and Prévost (2003)].

r_d/a	$K_1/\sigma\sqrt{\pi a}$	Error
0.283	1.033	2.68%
0.354	1.015	0.90%
0.424	1.004	-0.20%
0.566	1.005	-0.10%
0.707	1.005	-0.10%

Table 2: Normalized SIFs for the center crack problem (unstructured mesh with 3362 finite elements), Using XFEM: [Huang, Sukumar, and Prévost (2003)].

r_d/a	$K_1/\sigma\sqrt{\pi a}$	Error
0.424	1.0230	1.69%
0.573	1.0000	-0.60%
0.716	0.9920	-1.40%
0.859	0.9940	-1.20%

Table 3: Computational results by using SGBEM, for the center crack of Fig. 9

Mesh	Number of Nodes	$K_1/\sigma\sqrt{\pi a}$	Error
(a)	7	1.005	0.10%
(b)	12	1.006	0.00%
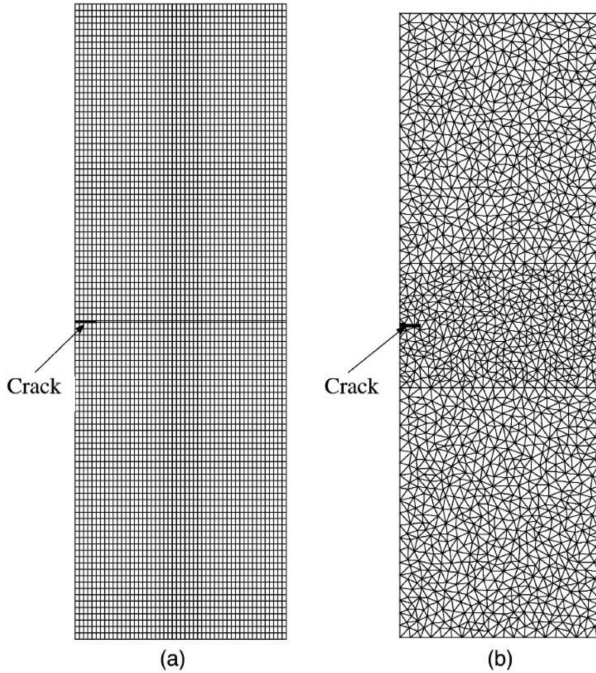
Figure 8: XFEM meshes for the center crack problem, taken from [Huang, Suku-mar, and Prévost (2003)]: (a) structured mesh with 5000 elements; (b) unstructured mesh with 3362 elements

Example 2. An Edge Crack

An edge crack of length a in a finite plate is shown in Fig. 10 with $b = h = 1$ and loaded by a uniform tensile stress $\sigma = 1$. [Tada, Paris, Irwin (2000)] gives:

$$\frac{K_1}{\sigma\sqrt{\pi a}} = 1.12 - 0.231\left(\frac{a}{b}\right) + 10.55\left(\frac{a}{b}\right)^2 - 21.72\left(\frac{a}{b}\right)^3 + 30.39\left(\frac{a}{b}\right)^4 \qquad (20)$$

This problem was solved by [Stazi, Budyn, Chessa, Belytschko, (2003)], using XFEM. The mesh of XFEM is shown in Fig. 11, with 484 linear as well as quadratic triangular elements. In this study, we also solve this problem with SGBEM, the mesh of which is shown in Fig. 12, with 35 boundary elements and 37 nodes. Computational results by XFEM, and the SGBEM, are shown and compared in Tab. 4, from which we see that the SGBEM gives much more accurate results than XFEM, with a much less computational cost.

(a)   (b)
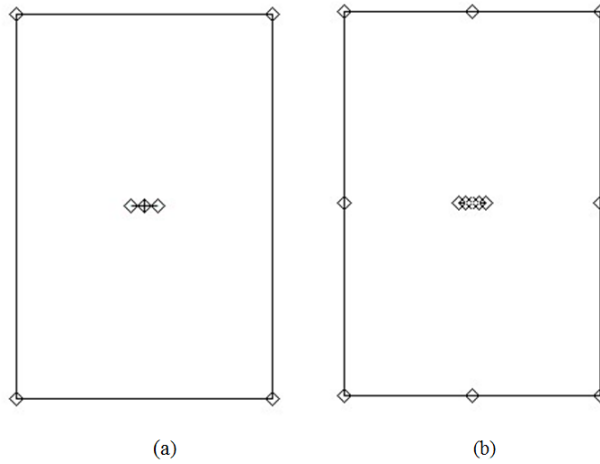
Figure 9: SGBEM meshes for the center crack problem: (a) with 6 elements, and a total of 7 nodes; (b) with 12 elements, and a total of 13 nodes;
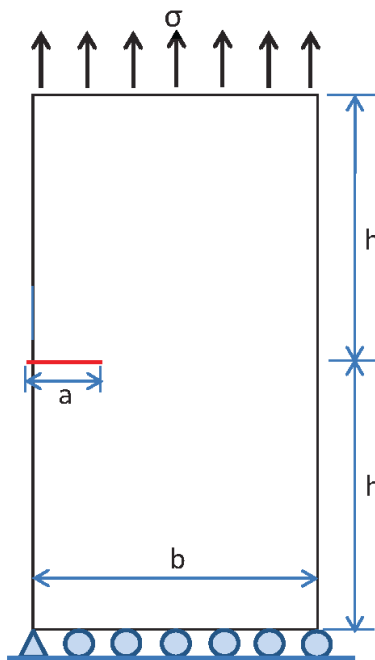
Figure 10: An Edge Crack

Table 4: Comparison of results by using XFEM [Stazi, Budyn, Chessa, Belytschko, (2003)], and by the present SGBEM, for the edge crack in Fig. 10,

a	Linear XFEM		Quadratic XFEM		SGBEM		Exact K_1
	K_1	error	K_1	error	K_1	error	
0.21	1.0616	-6.39%	1.1243	-0.86%	1.1296	-0.40%	1.1341
0.22	1.1000	-6.90%	1.1691	-1.05%	1.1767	-0.41%	1.1816
0.23	1.1321	-7.98%	1.2187	-0.94%	1.2252	-0.41%	1.2303
0.24	1.1558	-9.62%	1.2707	-0.63%	1.2751	-0.29%	1.2788
0.28	1.3783	-7.71%	1.4760	-1.17%	1.4911	-0.16%	1.4935
0.50	3.1299	-11.64%	3.5064	-1.01%	3.5302	-0.34%	3.5423
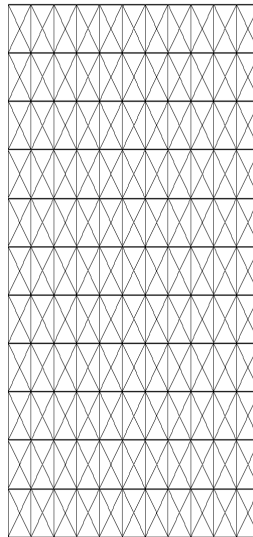
Figure 11: The XFEM mesh with 384 triangular elements
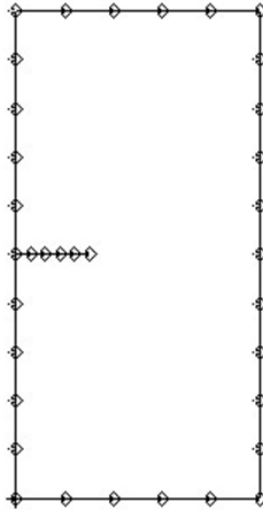
Figure 12: The present SGBEM mesh for the problem in Fig. 10, by using 35 boundary elements and 37 nodes

Example 3. An Embedded Slanted Crack

Now we solve the problem of an embedded slanted crack in an infinite domain, see Fig. 13. The coordinates of the two crack tips are $(-1, -0.9)$ and $(1, -0.9)$. Normal stress $\sigma = 1$ is applied in the vertical direction. This problem was solved by [Stazi, Budyn, Chessa, Belytschko, (2003)] with XFEM. The meshes of XFEM are similar to those in Fig. 11, but different number of elements were tried for this problem, by [Stazi, Budyn, Chessa, Belytschko, (2003)]. The results computed with XFEM for the upper-right crack-tip is shown in Tab. 5. We also solve this problem with SGBEM. A truncated plate with $b = h = 20$ is considered. The mesh of SGBEM is shown in Fig. 14, with 11 nodes for mesh (a), and with 21 nodes for mesh (b). Computed stress intensity factors with SGBEM are shown in Tab. 6, showing significantly higher accuracy than XFEM.

Example 4. A Branching Crack

We study the case of a branching crack in an infinite plate, with a=b=1, $\theta = 45°$, as shown in Fig. 15. Uniform stress $\sigma = 50$ is applied to the upper and lower edges.

This problem was studied by [Daux, Moës, Dolbow, Sukumar, Belytschko (2000)] with XFEM. Because of the limit of FEM, a truncated plate with w=20, H =16 was considered. The influence of the average element size h at the crack-tip on the
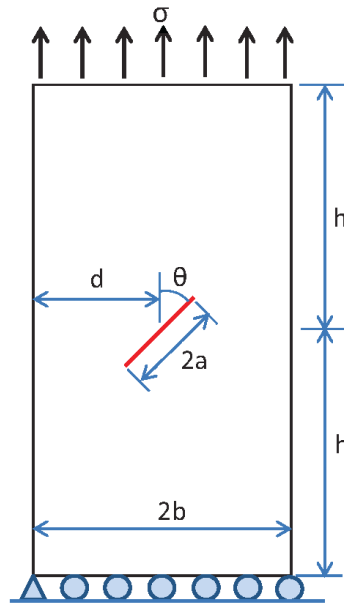
Figure 13: An Embedded Slanted Crack

Table 5: Results computed, using the XFEM, by [Stazi, Budyn, Chessa, Belytschko, (2003)]for the embedded slanted crack in Fig. 13

Number of Nodes	Error of K_1	Error of K_2
1661	33.53%	77.95%
2377	30.60%	27.22%
3449	-4.91%	-11.72%
4193	-2.88%	-6.73%
5293	-2.51%	-5.15%

Table 6: The results computed using the present SGBEM for the embedded slanted crack in Fig. 13

Number of Nodes	Error of K_1	Error of K_2
11	1.01%	1.03%
21	0.32%	0.33%

(a)   (b)
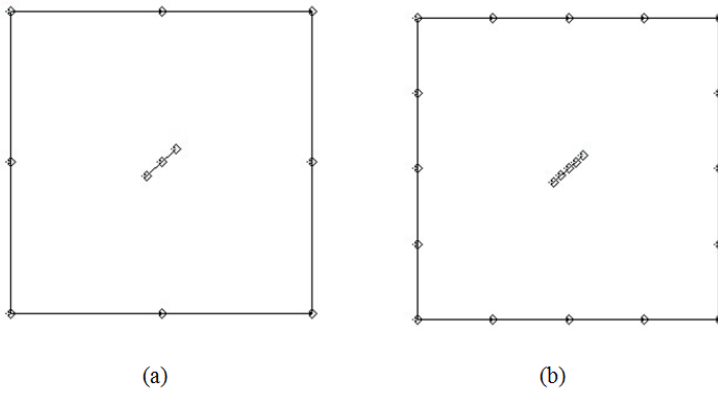
Figure 14: The SGBEM mesh for the slanted crack: (a) 10 boundary elements with 11 nodes; (b) 20 boundary elements with 21 nodes.
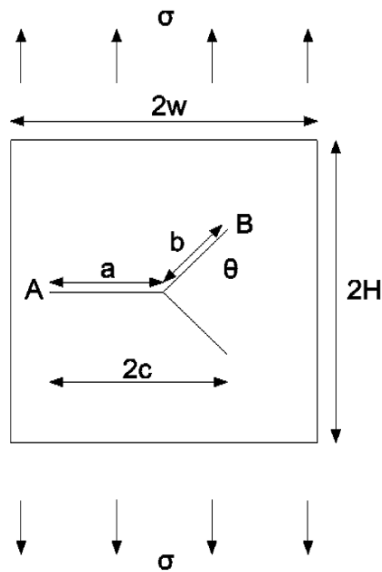
Figure 15: A branching crack

computed stress intensity factors is shown in Tab. 7. In order to obtain an accurate solution, extremely refined mesh at the crack tip was found to be necessary [Daux, Moës, Dolbow, Sukumar, Belytschko (2000)]. Therefore, if one wants to study the fatigue growth of the branching crack, even a finer mesh is necessary at the whole domain, in XFEM.

In Tab. 7, F_{1A}, F_{1B}, F_{2B} are defined as:

$$F_{1A} = \frac{K_{1A}}{\sigma\sqrt{\pi c}}$$

$$F_{1B} = \frac{K_{1B}}{\sigma\sqrt{\pi c}} \tag{21}$$

$$F_{2B} = \frac{K_{2B}}{\sigma\sqrt{\pi c}}$$

The XFEM results are compared to the reference solution of [Chen and Hasebe (1995)], which gives $F_{1A} = 1.044, F_{1B} = 0.495, F_{2B} = 0.506$.

(a)   (b)
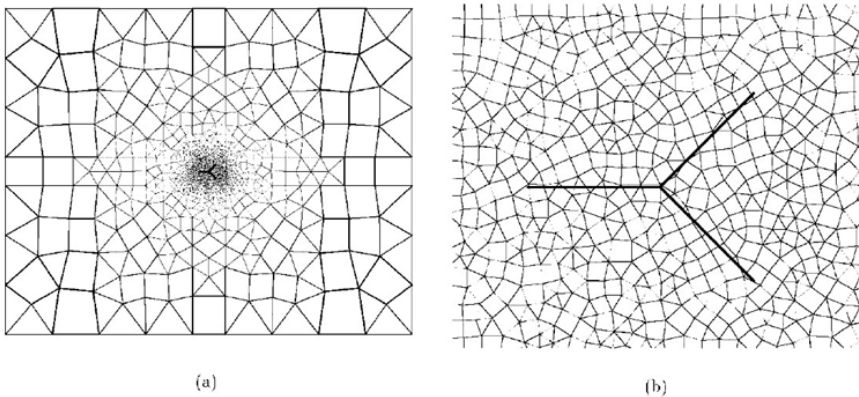
Figure 16: (a) XFEM mesh of the branching crack, with 1218 nodes, $h/a = 1/12$; (b) the close-up view of the mesh near the crack, taken from [Daux, Moës, Dolbow, Sukumar, Belytschko (2000)]:

This problem was also studied by SGBEM in [Dong and Atluri (2012a)], with $W/a = 40, H/a = 40$. The mesh for the SGBEM is shown in Fig. 17, with 46 boundary elements, and 49 nodes. The results computed by using the SGBEM are given in Tab. 8, showing high accuracy, even though a very coarse mesh is used. Moreover, the fatigue growth of the branching crack is also studied by SGBEM. In each crack-growth step, after computing stress intensity factors, the corresponding Eshelby-vector of force on the crack-tip (front) is determined by using its relation to

the mixed-mode SIFs, see [Nikishokv, Park and Atluri (2001)]. The crack-growth direction is taken to be the same as the direction of the Eshelby-vector of force, which has the physical meaning of "force on the singularity" [Eshelby (1951)]. The Paris equation: $da/dN = CK^n$ is used to determine the crack-growth rate, and the number of fatigue cycles required for a certain crack-length increment. The parameters of the equation are: $C = 6.9 \times 10^{-12}$ and n = 3. A maximum increment 0.3 is considered for crack tips in 30 crack-growth steps. The branching crack has grown to a final shape as shown in Fig. 18. This would be extremely difficult to achieve by using XFEM, since as shown in Tab. 7, an extremely refined mesh at the crack-tip is necessary. In order to perform an accurate fatigue analysis, which is easily achieved by SGBEM, in contrast, XFEM needs an extremely fine mesh over the whole domain.

We would like to emphasize that, with power-function types of fatigue laws (for example $da/dN = 6.9 \times 10^{-12} K^3$ as used in this example), a 10% error in SIFs can readily give 30%-40% errors in the number of estimated fatigue cycles. Surprisingly, we find that most of the XFEM studies in the literature do not list the computed numbers for fatigue cycles for a specified amount of crack-growth, in their studies. In many fatigue examples in this study, we list the computed numbers of fatigue cycles, and hope some comparison with XFEM for fatigue crack propagation will be provided by other researchers in the future.

Table 7: Results computed by using XFEM [Daux, Moës, Dolbow, Sukumar, Belytschko (2000)], for the branching crack in Fig. 15,

h/a	F_{1A}	error	F_{1B}	error	F_{2B}	error
0.40	0.963	-7.76%	0.460	-7.07%	0.458	-9.49%
0.30	1.009	-3.35%	0.468	-5.45%	0.464	-8.30%
0.22	1.027	-1.63%	0.498	0.60%	0.501	-0.99%
0.18	1.056	1.15%	0.493	-0.40%	0.506	0.00%
0.16	1.038	-0.57%	0.493	-0.40%	0.503	-0.59%
0.14	1.042	-0.19%	0.494	-0.20%	0.505	-0.20%
0.12	1.045	0.10%	0.493	-0.40%	0.504	-0.10%
0.10	1.045	0.10%	0.495	0.00%	0.507	0.20%
0.05	1.044	0.00%	0.496	0.20%	0.508	0.40%

Table 8: Results computed by using the present SGBEM, for the branching crack in Fig. 14

	SGBEM	Chen and Hasebe (1995)	Error
F_{1A}	1.044	1.044	0.00%
F_{1B}	0.494	0.495	0.20%
F_{2B}	0.507	0.506	0.20%

(a)   (b)
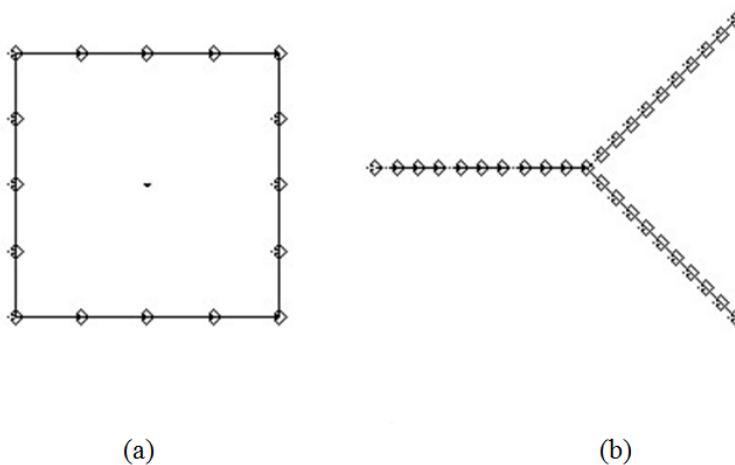
Figure 17: (a) The SGBEM mesh for the branching crack with 46 boundary elements and 49 nodes; (b) the close-up view of the crack
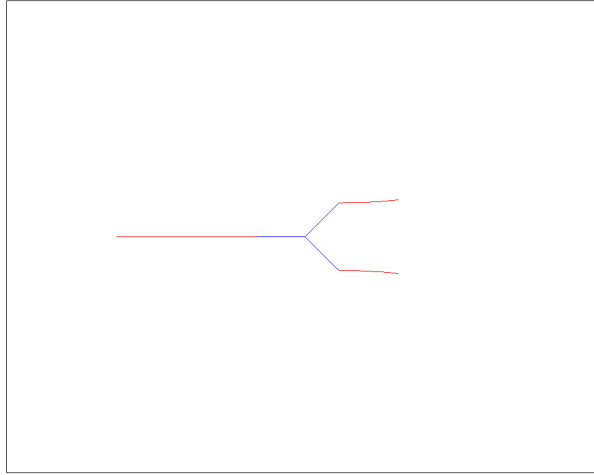
Figure 18: The shape of the branching crack of Fig. 15, after fatigue growth of 798159 cycles

Example 5. An Embedded Star-Shaped Crack

In this example, we consider a star-shaped crack as shown in Fig. 19. The geometrical parameters are: $\theta = 60°$, and H=w=4. Uniform stress $\sigma = 50$ is applied to each edge. In [Daux, Moës, Dolbow, Sukumar, Belytschko (2000)], it was found that the XFEM fails at $a/W \leq 0.1$. It was reported in [Daux, Moës, Dolbow, Sukumar, Belytschko (2000)] as: "*The SIF was not computed since the J-integral domain contained several crack tips*". This is expected, because XFEM needs a very fine mesh at the crack-tip. When the crack itself is very small compared to the global structure, it becomes very difficult to accurately compute the stress intensity factors, unless extremely fine mesh is used. However, SGBEM has no problem to model a very small crack. In this study, we consider an even smaller crack, $a = W/40$. The SGBEM mesh is shown in Fig. 20. A total of 76 elements and 82 nodes are used. F_{1A}, F_{1B} are defined as:

$$F_{1A} = \frac{K_{1A}}{\sigma\sqrt{\pi a}}$$

$$F_{1B} = \frac{K_{1B}}{\sigma\sqrt{\pi a}} \tag{22}$$

The results computed using the present SGBEM are shown in Tab. 9, and are in good agreement with those of [Chen and Hasebe (1995)].
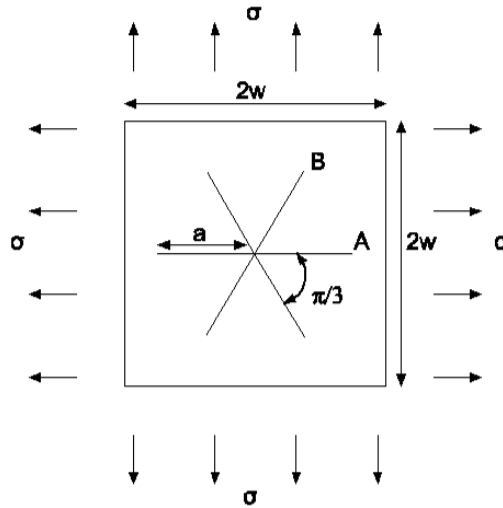
Figure 19: An embedded star-shaped crack

(a)   (b)
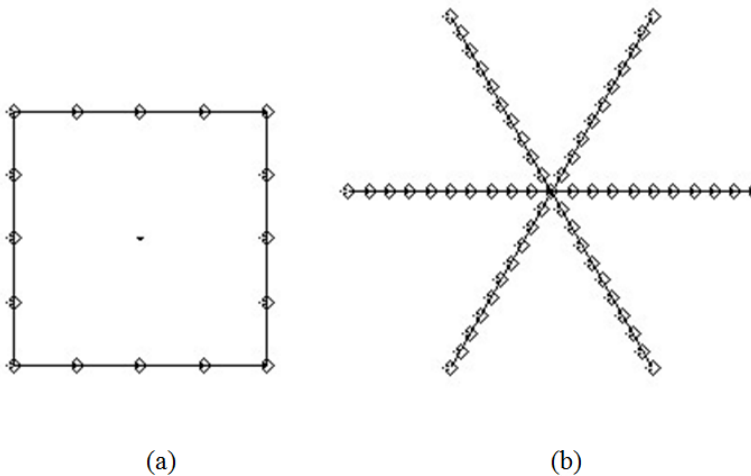
Figure 20: (a) The SGBEM mesh for the star-shaped crack, with 76 boundary elements and 82 nodes; (b) the close-up view of the crack

Table 9: Results computed by using the present SGBEM, for the star-shaped crack shown in Fig. 17

	SGBEM	Chen and Hasebe (1995)	Error
F_{1A}	0.743	0.743	0.00%
F_{1B}	0.743	0.743	0.00%

Moreover, the fatigue growth of the star crack was also studied by SGBEM. Paris equation: $da/dN = CK^n$ is used. The parameters of the equation are: $C = 6.9 \times 10^{-12}$ and n = 3. And a maximum increment 0.3 is considered for each crack tip, in a total 30 crack-growth steps. Computational results show that each segment of the star crack keeps growing in a straight line, and stays with the same shape, after 1,541,977 fatigue cycles, as shown in Fig. 21.
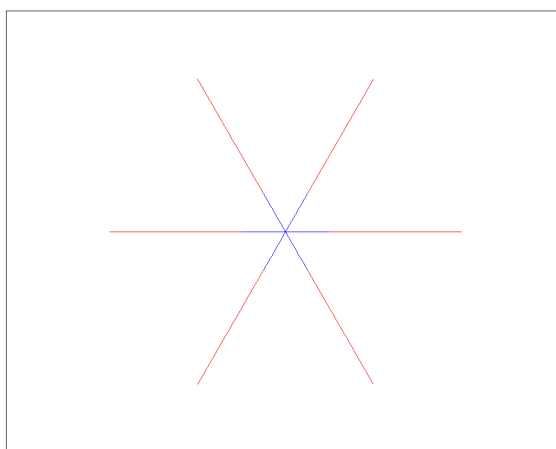
Figure 21: The shape of the star crack of Fig. 19, after growth under 1,541,977 fatigue cycles

Example 6. Two Off-Aligned Embedded Cracks

We solve the problem of a plate with two off-aligned embedded cracks, as shown in Fig. 22. The plate is 40×80. The two parallel cracks are with dimensions of a=1.27, e/f=0.3 and 2a/d=0.8. The crack without tip A is located at the center of

the plate. An evenly distributed tensile loading of 400 is applied to the upper and lower edges. A total of 50 elements and 52 nodes is used for the SGBEM mesh. K1 for crack tip A is compared to the Handbook solution [Murakami (1987)] in Tab. 10.

Moreover, the fatigue growth of these two off-aligned cracks is also studied by SGBEM. The Paris equation: $da/dN = CK^n$ is used with C = 6.9×10^{-15}. Three different values are used for n: (a) $n = 3$; (b) $n = 1$; (c) $n = 0$. Smaller values of n indicate a smaller influence of SIFs on the crack-growth rates. In the limit of $n = 0$, crack-growth rates are irrelevant to SIFs, and all the crack tips grow at the same speed. A maximum increment 6 is considered for each crack tip, in a total 30 crack-growth steps. The predicted final crack shape after fatigue growth is shown in Fig. 24-26. It is interesting to see the influence of n on the final crack shapes.
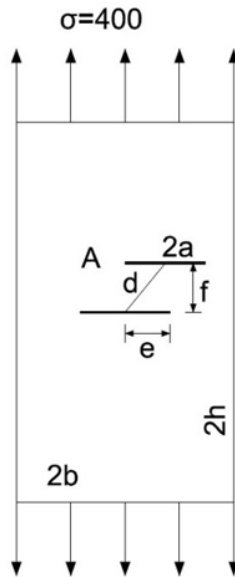
Figure 22: Two off-aligned embedded cracks

Table 10: Computational results for the two off-aligned cracks in Fig. 22

	SGBEM	Handbook	Error
K_{1A}	673.140	671.144	0.30%

(a)   (b)
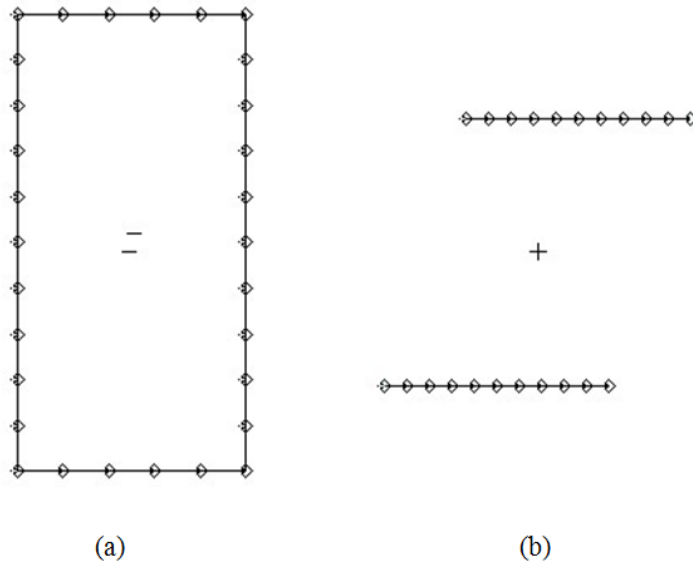
Figure 23: (a) The SGBEM mesh for the two embedded off-aligned cracks, with 50 boundary elements and 52 nodes; (b) the close-up view of the crack
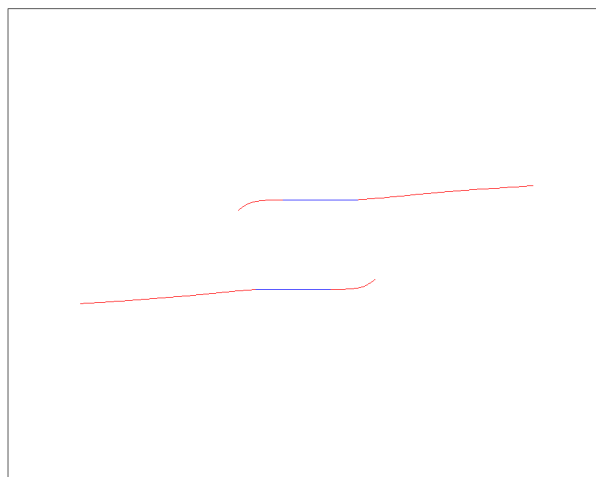
Figure 24: The shapes of the two off-aligned cracks of Fig. 22, after growth under 4.7×10^5 cycles, considering $da/dN = 6.9 \times 10^{-15} K^3$
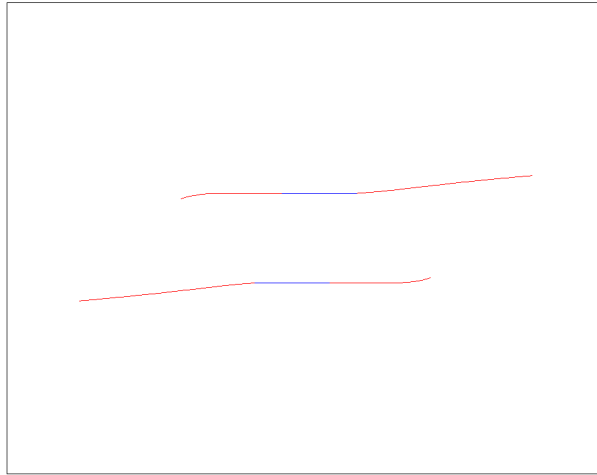
Figure 25: The shapes of the two off-aligned cracks of Fig. 22, after growth under 6.5×10^{11} cycles, considering $da/dN = 6.9 \times 10^{-15} K^1$
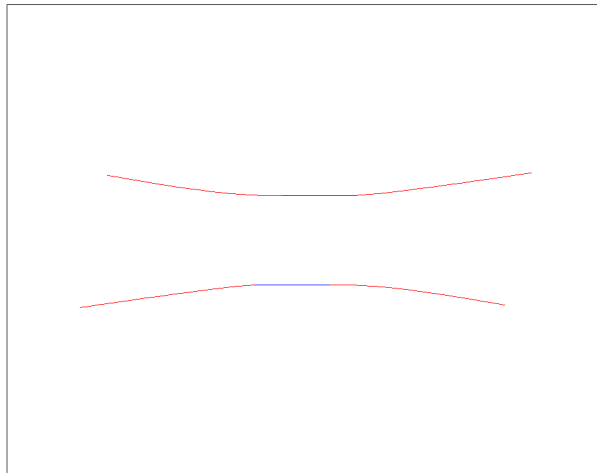
Figure 26: The shape of the two off-aligned cracks of Fig. 22, after growth under 8.7×10^{14} cycles, considering $da/dN = 6.9 \times 10^{-15} K^0$

Example 7. Three Embedded Parallel Cracks

Another example is selected: three parallel cracks are aligned normally to the tensile direction. A schematic of the problem is shown below in Fig. 27. The plate is 40×80. The three parallel cracks are with dimensions of a=1.27, d=3.175. The crack B is located at the center of the plate. An evenly distributed tensile loading of 400 is applied to the upper and lower edges. A total of 60 elements and 63 nodes is used, as shown in Fig. 28. SIFs for crack tips A and B are compared to the Handbook solution [Murakami (1987)] in Tab. 11. The fatigue growth of these three parallel cracks is also studied by SGBEM. Paris equation: $da/dN = CK^n$ is used with $C = 6.9 \times 10^{-15}$ and $n = 3$. A maximum increment 6 is considered for each crack tip, in a total 30 crack-growth steps. The predicted final crack shape after fatigue growth is shown in Fig. 29.
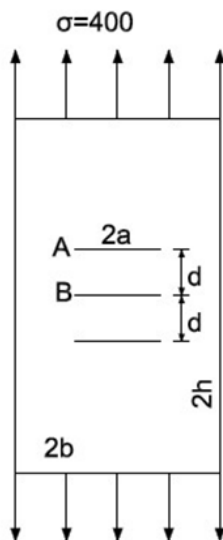
Figure 27: Three parallel cracks

Table 11: Computational results for the three parallel cracks as shown in Fig. 27

	SGBEM	Handbook	Error
K_{1A}	681.802	679.550	0.38%
K_{1B}	602.97	599.235	0.62%
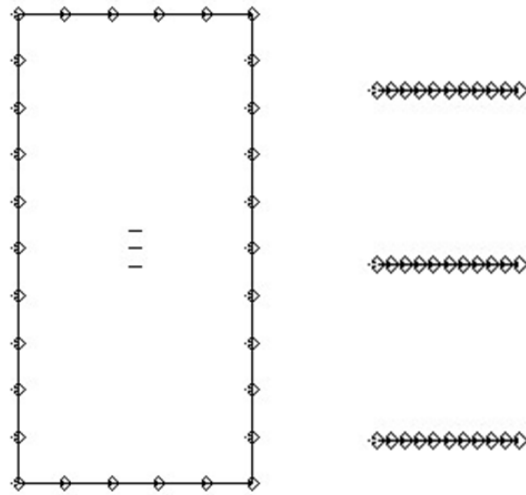
Figure 28: (a) The SGBEM mesh for the three parallel cracks, with 60 boundary elements and 62 nodes; (b) the close-up view of the crack
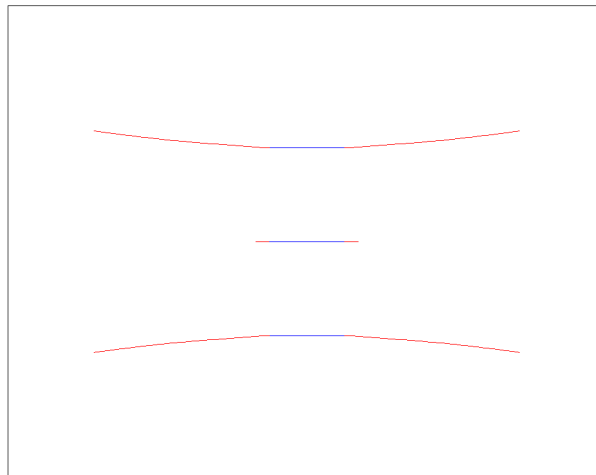
Figure 29: The shapes of the three embedded parallel cracks of Fig. 27, after growth under 662,872 fatigue cycles

Example 8. The Merging of Two Embedded Slanted Cracks Under Fatigue

In this example, we demonstrate the merging of two embedded slanted cracks. The same plate as in Example 4 for a branched crack, as shown in Figure 15, is used. However, the segments of the branched crack, for x < 0.02, in Fig. 14 are eliminated, so that the remaining parts involve two slanted cracks, as shown in Fig. 30. Biaxial tension σ=50 is applied. The mesh of the plate with slanted cracks is shown in Fig. 30, with 36 boundary elements and 38 nodes. The fatigue growth of these two slanted cracks is also studied by SGBEM. The Paris equation: $da/dN = CK^n$ is used with C = 6.9 × 10^{-12} and $n = 0$. A maximum increment of 0.3 is considered for each crack tip, in a total 50 crack-growth steps. The predicted final crack shapes after fatigue growth are shown in Fig. 31.
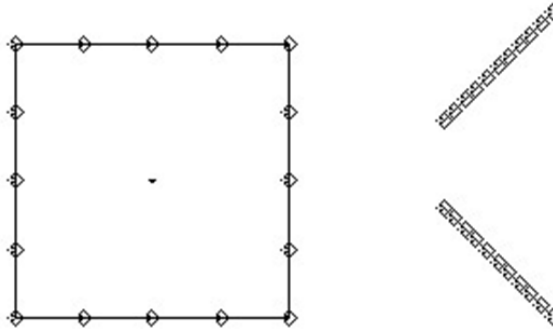
Figure 30: (a) The SGBEM mesh for the two slanted cracks, with 36 boundary elements and 38 nodes; (b) the close-up view of the crack

Example 9. Very Small Cracks near A Fastener Hole

In this example, very small edge cracks emanating from a circular fastener hole are considered. A schematic of the problem is shown in Figure 32. The plate is 50.8×101.6. A circular hole with R=6.35 is located at the center of the plate, and cracks emanate from the hole. The length of each small crack is 0.254, which is only 2% of the diameter of the fastener hole. Thus the summation of the radius and the crack length is. $a = 6.604$. An evenly distributed tensile loading of 82.74 is applied to the upper and lower edge. The SGBEM mesh of this problem is shown in Fig. 33. A total of 84 boundary elements and 87 nodes are used. The computational results are compared to the handbook solution of [Murakami (1987)] in Tab. 12.
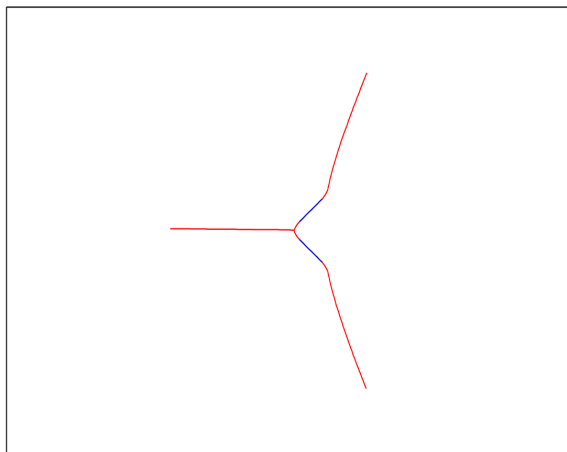
Figure 31: The shapes of the two slanted cracks of Fig. 30, after growth under 4.3×10^{10} cycles
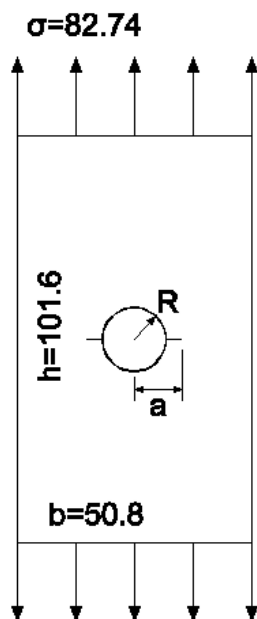
Figure 32: Cracks from a Circular Fastener Hole
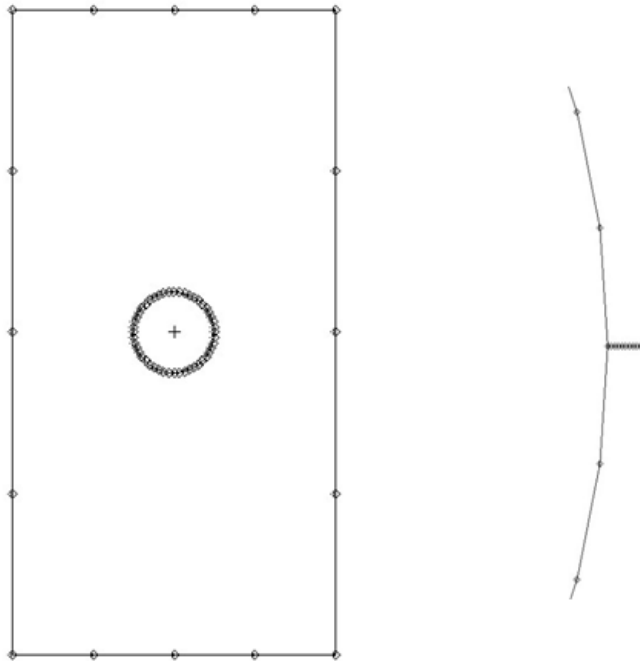
Figure 33: (a) The SGBEM mesh for the problem with two very small cracks near a fastener hole, with 84 boundary elements and 86 nodes; (b) the close-up view of the crack

Table 12: Computational Results for the cracks in Fig. 32, obtained through SGBEM

	SGBEM	Handbook	Error
K_1	249.55	248.47	0.43%
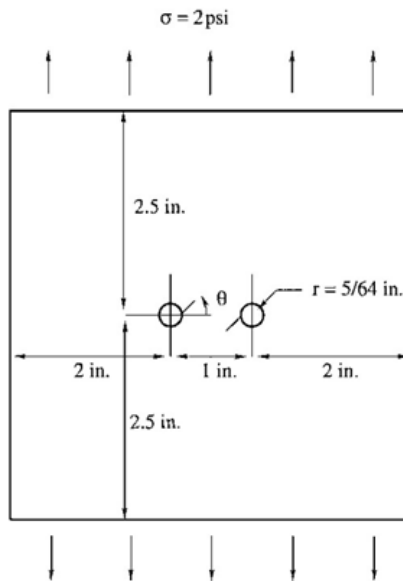
Figure 34: Slanted cracks emanating from loaded fastener holes, taken from [Moës, Dolbow and Belytschko (1999)]
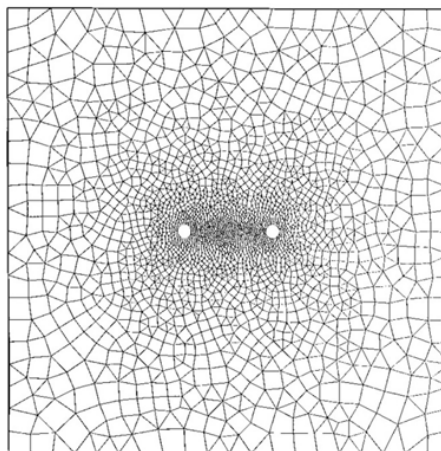
Figure 35: "The Coarse mesh" used by XFEM, taken from [Moës, Dolbow and Belytschko (1999)], for the problem in Fig. 34

Example 10. Fatigue Growth of Cracks Emanating from Fastener Holes

We also model the mixed mode fatigue growth of multiple slanted cracks emanating from fastener-holes in an aircraft fuselage lap-joint. Fig. 34 shows the geometry of the plate with the two holes and the cracks emanating from them. In the initial configuration, both the cracks have a length of 0.1 in and are oriented at angles $\theta = 45°$ and -45° for the left and right holes, respectively.

The fatigue growth of the cracks emanating fastener holes was studied by [Moës, Dolbow and Belytschko (1999)] using XFEM. Two meshes were used in XFEM: a "coarse mesh" with 2650 finite elements as shown in Fig. 35, and a "fine mesh" which was not shown in their original paper and thus not shown here. The crack shape after fatigue growth is shown in Fig. 36. Some discrepancies of the results by the "coarse mesh" and the "fine mesh" can be observed, where some obvious kinks are present in the crack path obtained by using the "coarse mesh".

Figure 36: The final shapes of cracks emanating from fastener holes after fatigue growth by XFEM, taken from [Moës, Dolbow and Belytschko (1999)]

This problem is also modeled by SGBEM in this study. The SGBEM mesh is shown in Fig. 37, with 102 elements and 106 nodes. The predicted crack paths are shown in Fig. 38, which are very smooth without kinks, as compared to those by XFEM.

Example 11. Growth and Intersection of Densely Distributed Cracks

In this section, we study the growth and intersection of 25 densely distributed small cracks, under remote tension. A 0.5×0.5 plate is considered. A close-up view of a 0.05×0.05 region with distributed cracks is shown in Fig. 39. Uniform tension is applied to each edge of the plate. When cracks grow, some tend to grow into others. When one crack grows into another crack (see Fig. 40), we consider that it does not go any further, and the intersection-point is specially treated by appending a constraint of balance of dislocations, as discussed in [Dong and Atluri (2012)]. The crack pattern after fatigue growth is shown in Fig. 41. We should point out that, in [Huang, Sukumar, and Prévost (2003)], a similar analysis was performed.

(a)   (b)
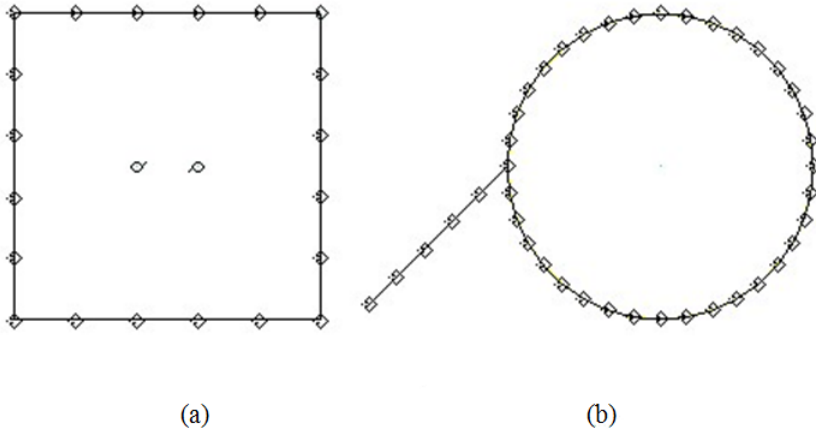
Figure 37: (a) The present SGBEM mesh for the cracks emanating from fastener holes, with 102 boundary elements and 106 nodes; (b) the close-up view of the crack
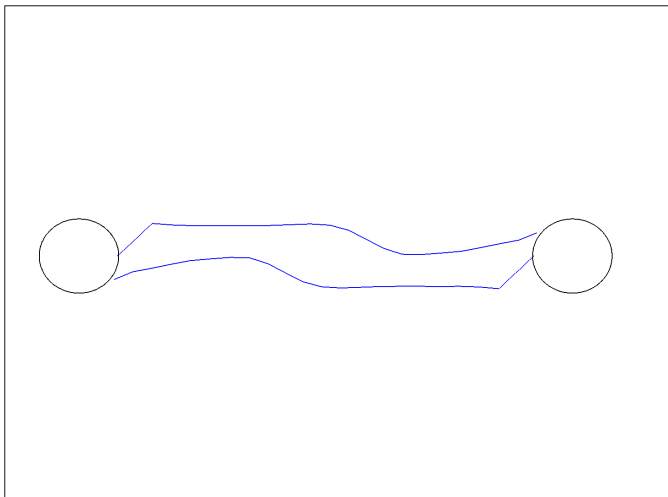
Figure 38: The final shapes of cracks emanating from fastener holes after fatigue growth, solved by the present SGBEM

However, in their study, if one crack grows very close to another, it is forced to stop growing and the crack-tip stays stationary at a location very close to the surface of another crack. This assumption is physically unrealistic; a branch-shaped pattern is expected to be formed, and should be specially treated, as shown in Fig.38. *We also would like to point out that, the computation of this complex example by SGBEM only takes 78 seconds on the PC mentioned before, showing the very high efficiency of the present SGBEM-based methods.*
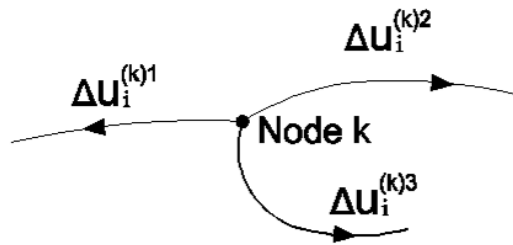
Figure 39: Treatment of the intersection point by appending the constraint $\Delta u_i^{(k)1} + \Delta u_i^{(k)2} + \Delta u_i^{(k)3} = 0$
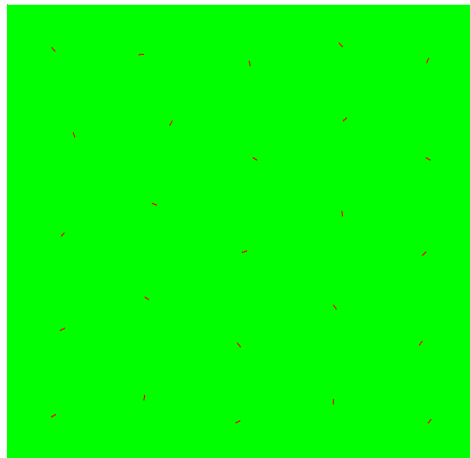
Figure 40: The initial configuration of 25 densely distributed small cracks
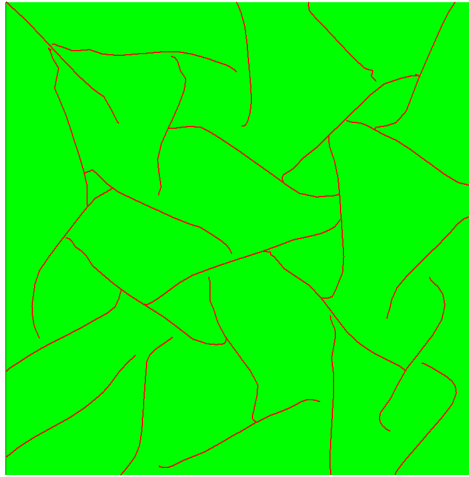
Figure 41: The final pattern after fatigue growth of cracks (Using the present SGBEM-based method)

Example 12. Fatigue Analysis of Stiffened Aircraft Panels with Composite-Patches

In this example, we use SGBEM in combination with FEM to analyze the fatigue growth of a center crack in a thin panel, with/without stiffeners and/or composite patches. And as far as the authors know, the XFEM approach was never found to be able to perform such an analysis.

Four cases are considered:

Case (a): panel without stiffeners or any composite patch

Case (b): panel with 2 stiffeners only

Case (c): panel with 1 composite patch only

Case (d): panel with 2 stiffeners and 1 composite patch

A 250mm by 500mm panel is considered. A crack with initial length 25.7mm is located in the center of the panel. The length of each stiffener is 400 mm, and they are separated by a distance of 140 mm. The dimensions of the composite patch are 70mm by 100mm. The fibers of the composite patch are laid in the same direction of the tension applied to the upper and lower edges.

Material properties are considered as:

Isotropic material for Panel: E=72.4 GPa, v=0.32, t =1mm.

Isotropic material for adhesive layer: E=1.07 GPa, v=0.32, t =0.127mm.

Orthotropic material for patch: E_1=210 GPa, E_2=25 GPa, G_{12}=7.2 GPa, v_{12}=0.17, t=0.381mm.

Stiffeners: E=72.4 GPa, A=130 mm^2, I =4370mm^4.

(a)   (b)
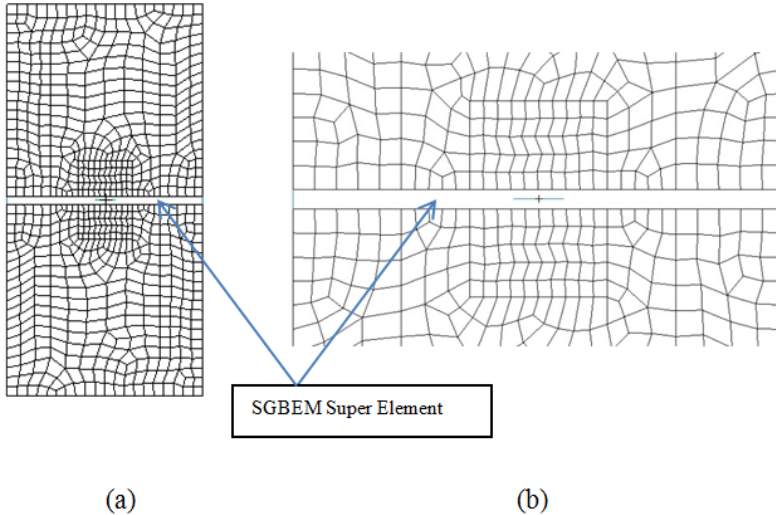
Figure 42: (a) Mesh for the plate with center crack by using quadrilateral elements and a Super Element, (b) a close-up view of the SGBEM Super Element

The meshes of the panel, adhesive, patch and stiffeners are shown in Fig. 42-44. The panel is modeled with quadrilateral elements and one Super Element. The adhesive layer and the composite patch are modeled using quadrilateral elements. And the stiffeners are modeled by beam elements, with both translational and rotational degrees of freedoms.

A maximum uniform tension of 120Mpa is applied to the upper and the lower edge of the panel. Stress ratio of 0.1 is considered. Paris equation: $da/dN = CK^n$ is used. The parameters of the equation are: C = 5.85×10^{-14} and n = 3.59 (with *Newton − mm* units). The number of analysis steps is 40. The total crack increment =40mm (for each tip). So in each step the crack increment is 1mm. Predicted loading cycles are plotted against crack lengths in Fig. 45. As shown in the results, the order of the magnitude of fatigue lives for each case is such that: (d)>(c)>(b)>(a), which is as expected.
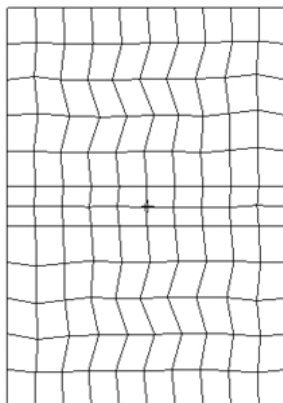
Figure 43: Mesh for the composite patch and the adhesive layer by using quadrilateral elements
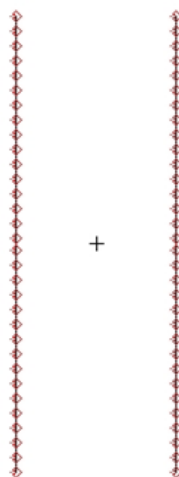
Figure 44: Mesh for the stiffeners by using beam elements
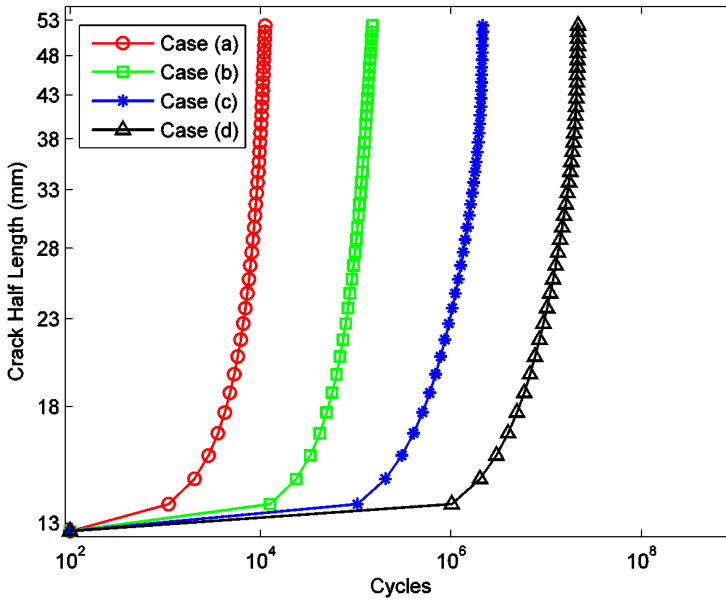
Figure 45: Predicted fatigue lives for the crack panel

Example 13. Interaction of A Microcrack with Inclusions and Voids

In this section, the interactions between a microcrack and inclusions/voids are studied by SGBEM.

To the best knowledge of the authors, there has not been any quantitative analysis of the stress intensity factors of a microcrack near an inclusion. Therefore, we firstly model this problem, see Fig. 46. A truncated 200×200 finite plate is considered. The radius of the inclusion is $r_v = 5$. The length of the crack is $2a_v = 10$. The properties of the matrix material are $E_m = 1, v_m = 0.35$. The properties of the inclusion are $E_c = 22.15, v_c = 0.3$. The center point of the crack is at $(2.5, 10)$. ***A single SGBEM Super Element is used to solve this problem***. This example has been studied by [Hwu, Liang and Yen (1995), Williams, Phan, Tippur, Kaplan and Gray (2007)]. In Tab. 13, we compare the presently computed normalized stress intensity factor, to the analytical solution in [Hwu, Liang and Yen (1995)] :

$$F = \frac{K}{\sigma\sqrt{\pi a_v}} \tag{23}$$

In the next example, we model the fatigue growth of a crack passing an inclusion. The geometry of this problem is shown in Fig. 47. A 4×4 plate is considered. A

Table 13: The stress intensity factors of the micro-crack near an inclusion, for the problem in Fig. 46

	SGBEM	Analytical
F_{1A}	0.833	0.834
F_{2A}	-0.062	-0.062
F_{1B}	0.916	0.915
F_{2B}	-0.052	-0.052
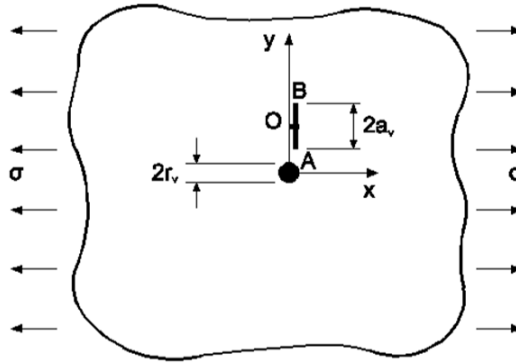
Figure 46: Crack / inclusion interaction in an infinite plate, analyzed by the present SGBEM-based SVC

circular inclusion with radius 0.25 is placed in the center. An edge crack with initial length 1.5 is considered. The material properties of the matrix are $E_m = 1, v_m = 0.3$. The material properties of the inclusion are $E_c = 3, v_c = 0.3$. A uniform tension is applied to the upper and lower edges of the plate. *A single SGBEM super element with an inclusion and a crack is used to solve this problem*. After fatigue growth, the crack is deflected by the inclusion, and then continues to grow into a mode 1 dominated crack, as shown in Fig. 48.

In a companion example, the same geometry in Fig. 47 is considered. However, this time a hole is considered instead of an inclusion. The material properties are $E = 1, v = 0.3$. Unlike the shielding effect of stiffer inclusion, the crack in this example eventually grows into the hole and stops, as can be seen in Fig. 49.

We also model the growth of a microcrack near two inclusions or two holes. The geometry of this problem is shown in Fig. 50. A 4×4 plate is considered. Two circular inclusions or holes with radius 0.25 are placed symmetrically in the upper
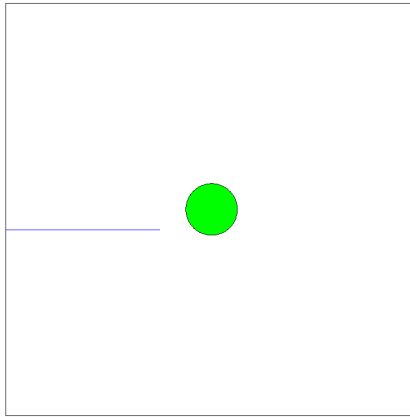
Figure 47: Initial crack near the inclusion or hole, analyzed by the present SGBEM-based SVC
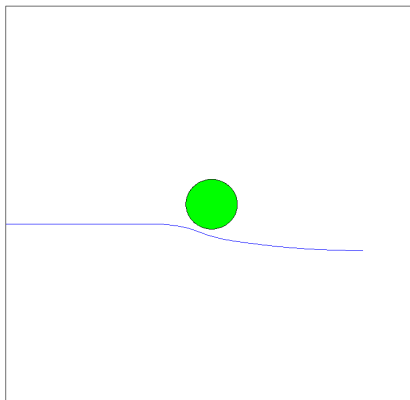
Figure 48: The final shape of the microcrack, after growing in fatigue, and after being deflected by the inclusion, analyzed by the present SGBEM-based SVC
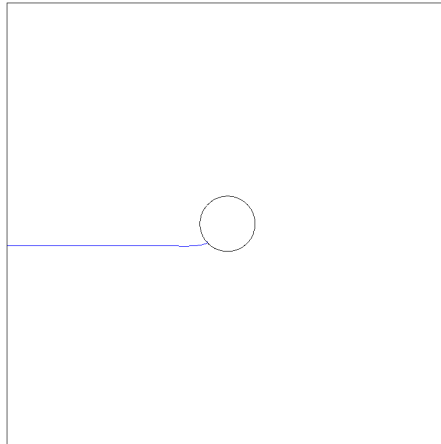
Figure 49: Final shape of the micro-crack, after fatigue: Crack grows into the void (analyzed by the present SGBEM-based SVC)
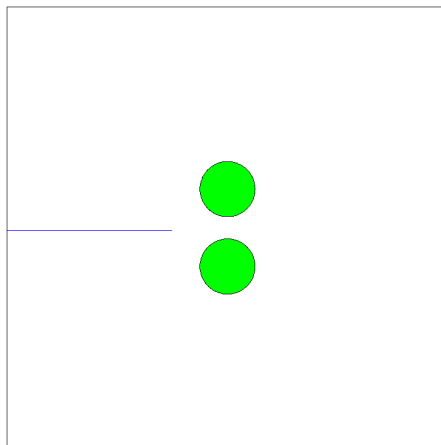
Figure 50: slightly eccentric micro crack near two inclusions or two voids (analyzed by the present SGBEM-based SVC)
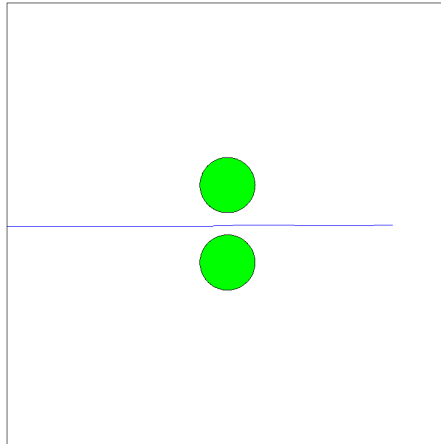
Figure 51: final shape of the micro-crack, after growing under fatigue, and after passing through the two inclusions (analyzed by the present SGBEM-based SVC)
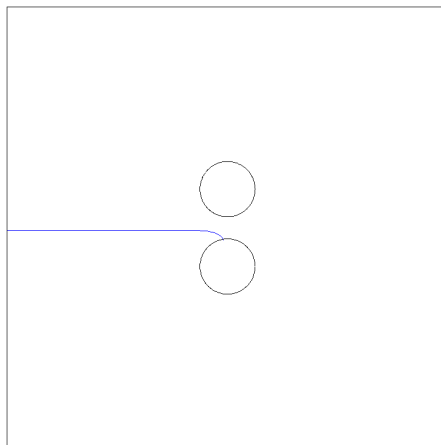
Figure 52: Final shape of the micro crack, after growing under fatigue, and after growing into one of the two holes (analyzed by the present SGBEM-based SVC)

and lower part of the plate. The distance between the two inclusions is 0.2. An edge crack with initial length 1.5 is considered. The crack is slightly closer to the lower hole or inclusion. The distance between the initial crack and the mid-line of the plane is 0.02. The material properties of the matrix are $E_m = 1, v_m = 0.3$. The material properties of the inclusion are $E_c = 3, v_c = 0.3$. A uniform tension is applied to the upper and lower edges of the plate.

After fatigue growth, the final crack shapes are shown in Fig. 51-52. As can be seen clearly, the two stiffer inclusions push the crack back closer to the mid-line, and the crack successfully passes through the two inclusions. On the other hand, although the crack is only slightly eccentric, it grows into the nearer hole and stops.

Example 14. Microcracks in Composite Material

(a)   (b)
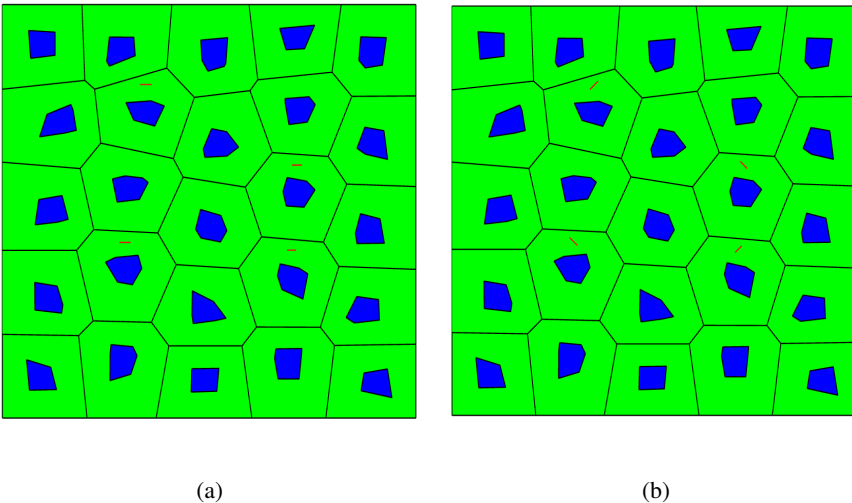
Figure 53: A RVE of Al/SiC material with 10% SiC, with: (a) horizontal microcracks; (b) inclined microcracks (analyzed by the present SGBEM-based SVC)

For the last example, we study the microcrack growth in Al/SiC material. A RVE of Al/SiC, with 10% SiC is used. Some microcracks are randomly generated in the RVE. As shown in Fig. 53, two cases are considered: (a), all microcracks are perpendicular to the loading direction; (b) microcracks are randomly inclined. The fatigue growth of these microcracks is considered, with a simple Paris Law: $da/dN = 6.9 \times 10^{-12} K^3$, with *Newton − mm* units. After fatigue growth of microcracks, the final crack shapes and the principal stress/strain energy density of case

(a) and case (b) are presented in Fig. 54-59. We see that, the fatigue growth of microcracks is clearly affected by the micro-structure: some cracks growth much faster than others. On the other hand, since the initial microcracks are very small, the inclination angle does not significantly affect the crack path.
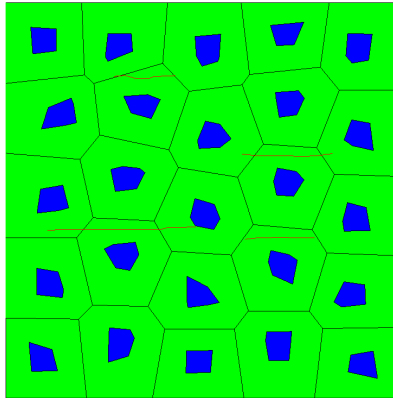
Figure 54: Final shapes of initially horizontal microcracks in Al/SiC material, after fatigue growth (analysed by the present SGBEM-based SVC)
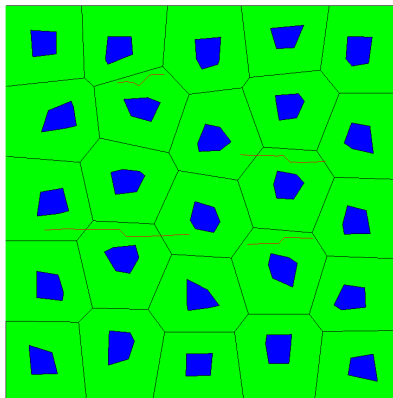
Figure 55: The final crack-shapes of initially inclined microcracks in Al/SiC material, after fatigue growth (analyzed by the present SGBEM-based SVC)
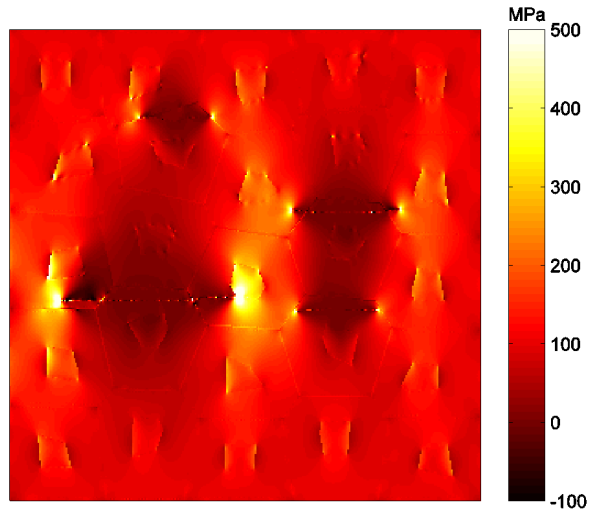
Figure 56: The distribution of maximum principal stress in an Al/SiC material with initially horizontal microcracks, after fatigue growth (analyzed by the present SGBEM-based SVC)
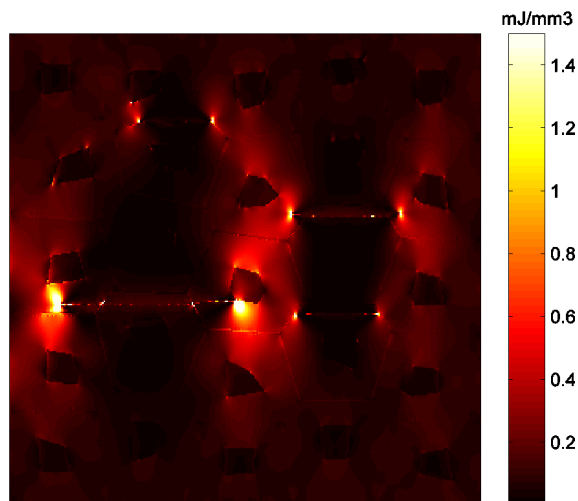
Figure 57: Distribution of strain energy density in Al/SiC material with initially horizontal microcracks, after fatigue growth (analyzed by the present SGBEM-based SVC)
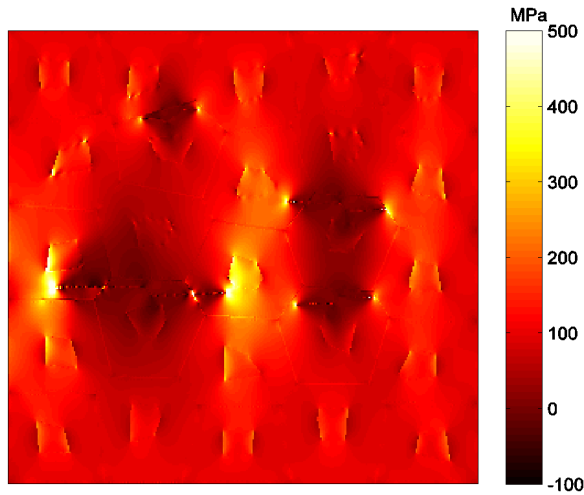
Figure 58: The distribution of maximum principal stress in an Al/SiC material with initially inclined microcracks, after fatigue growth (analyzed by the present SGBEM-based SVC)
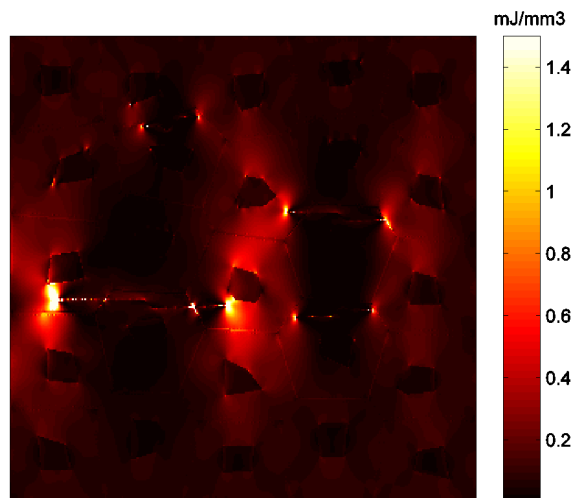
Figure 59: The distribution of strain energy density in an Al/SiC material with initially inclined microcracks, after their fatigue growth (analyzed by the present SGBEM-based SVC)

5 Conclusion

After a brief review of the historical developments, and the theoretical as well as algorithmic formulations, of both the XFEM and SGBEM-based methods, a careful and comprehensive examination of their suitability in fracture and fatigue analyses is presented. The many numerical examples presented in this paper show that, the SGBEM-based methods: (a) are far more accurate than XFEM, for computing stress intensity factors, and hence the fatigue crack-growth rates and fatigue lives; (b) require significantly coarser and lower-quality meshes than XFEM, and thus require significantly less computational cost and human labor costs; (c) require very minimal efforts for carrying out fatigue growth analyses of non-collinear/non-planar cracks, without having to use Level Set or Fast Marching method as is commonly done in XFEM, to track the crack surface; (d) can easily perform fracture and fatigue analysis of complex structures, such as cracked stiffened metallic panels with composite patch repairs, and microcracks in heterogeneous materials. It is thus concluded that the SGBEM-based methods, and alternating methods, which were developed over the last 20-30 years by Atluri and his many collaborators, are still by far the best methods for analyzing fracture and non-planar fatigue crack propagation in complex structures, and are thus valuable for inclusion in general-purpose, off-the-shelf commercial software for structural analyses. This objective is pursued by the authors.

Acknowledgements

References:

Atluri, S. N. (2005): *Methods of Computer Modeling in Engineering and the Sciences, Vol. 1*, Tech Science Press.

Atluri, S. N.; Kobayashi, A. S.; Nakagaki M. (1975): An assumed displacement hybrid finite element model for linear fracture mechanics, *International Journal of Fracture*, vol. 11, no. 2, pp. 257-271.

Atluri, S. N. (1986): *Computational Methods in the mechanics of fracture*, North Holland, Amsterdam (also translated into Russian, Mir Publishers, Moscow).

Atluri, S. N. (1998): *Structural Integrity and Durability*, Tech Science Press, Forsyth.

Bonnet, M.; Maier, G.; Polizzotto, C. (1998) Symmetric Galerkin boundary element methods. *Applied Mechanics Review*, vol. 51, pp. 669-704.

Barsoum, R. S. (1976). On the use of isoparametric finite elements in linear fracture mechanics. *International Journal for Numerical Methods in Engineering*, Vol. 10, issue 1, pp. 25-37.

Chen, Y. Z.; Hasebe, N. (1995): New integration scheme for the branch crack problem. *Engineering Fracture Mechanics,* vol. 52, no. 5, pp. 791-801.

Chen, F. H.; Shield, R. T. (1977): Conservation laws in elasticity of the J-integral type. *Zeitschrift für angewandte Mathematik und Physik ZAMP*, vol.28 issue 1, pp. 1-22.

Daux, C.; Moës, N.; Dolbow, J.; Sukumar, N.; Belytschko, T. (2000): Arbitrary branched and intersecting cracks with the extended finite element method. *International Journal for Numerical Methods in Engineering*, vol. 48, pp. 1741-1760.

Dong, L.; Atluri, S. N. (2012): SGBEM (Using Non-hyper-singular Traction BIE), and Super Elements, for Non-Collinear Fatigue-growth Analyses of Cracks in Stiffened Panels with Composite-Patch Repairs. CMES: *Computer Modeling in Engineering & Sciences*, vol.89, no. 5, pp. 417-458.

Dong, L.; Atluri, S. N. (2013a): SGBEM Voronoi Cells (SVCs), with Embedded Arbitrary-Shaped Inclusions, Voids, and/or Cracks, for Micromechanical Modeling of Heterogeneous Materials. CMC: *Computers, Materials & Continua*, In Press.

Dong, L.; Atluri, S. N. (2013b): Fracture & Fatigue Analysis: SGBEM-FEM or XFEM? Part 2: 3D Solids. CMES: *Computer Modeling in Engineering & Sciences*, In Press.

Eshelby, J. D. (1951): The Force on an Elastic Singularity. *Philosophical Transactions of the Royal Society A: Mathematical, Physical & Engineering Sciences,* vol. 244, no. 877, pp. 87-112.

Frangi, A; Novati, G. (1996): Symmetric BE method in two-dimensional elasticity: evaluation of double integrals for curved elements, *Computational Mechanics*, vol. 19, issue 2. pp. 58-68.

Frangi, A; Novati, G.; Springhetti, R.; Rovizzi, M. (2002): 3D fracture analysis by the symmetric Galerk in BEM, *Computational Mechanics*, vol. 28, pp. 220-232.

Gravouil, A.; Moës, N.; Belytschko, T. (2002). Non-planar 3D crack growth by the extended finite element and level sets-Part II: Level set update. *International Journal for Numerical Methods in Engineering*, vol. 53, issue 11, pp. 2569-2586.

Han, Z. D.; Atluri, S. N. (2002): SGBEM (for Cracked Local Subdomain) – FEM (for uncracked global Structure) Alternating Method for Analyzing 3D Surface Cracks and Their Fatigue-Growth. CMES: *Computer Modeling in Engineering*

& Sciences, vol.3, no.6, pp.699-716.

Han, Z. D.; Atluri, S. N. (2003): On Simple Formulations of Weakly-Singular Traction & Displacement BIE, and Their Solutions through Petrov-Galerkin Approaches. CMES: *Computer Modeling in Engineering & Sciences*, vol. 4, no. 1, pp.5-20.

Han, Z. D.; Atluri, S. N. (2007): A systematic approach for the development of weakly-singular BIEs. CMES*: Computer Modeling in Engineering & Sciences*, vol. 21, issue 1, 41-52.

Henshell, R. D.; Shaw, K. G. (1975): Crack tip finite elements are unnecessary. *International Journal for Numerical Methods in Engineering* vol. 9, issue 3, pp. 495-507.

Hong, H. K.; Chen, J. T. (1988): Derivations of integral equations of elasticity. Journal of Engineering Mechanics, vol. 114, issue 6, pp. 1028-1044.

Huang, R.; Sukumar, N.; Prévost, J. H. (2003): Modeling quasi-static crack growth with the extended finite element method Part II: Numerical applications. *International Journal of Solids and Structures*, vol. 40, issue 26, pp. 7539-7552.

Hwu, C.; Liang, Y. K.; Yen, W. J. (1995). Interactions between inclusions and various types of cracks. *International Journal of Fracture*, vol. 73, no. 4, pp. 301-323.

Li, S.; Mear, M.E.; Xiao, L. (1998): Symmetric weak form integral equation method for three-dimensional fracture analysis. *Computer Methods in Applied Mechanics and Engineering*, vol. 151, pp. 435-459.

Moës, N; Dolbow J; and Belytschko T. (1999): A finite element method for crack growth without remeshing. *International Journal for Numerical Methods in Engineering*, vol. 46, pp. 131-150.

Moës, N.; Gravouil, A.; Belytschko, T. (2002). Non-planar 3D crack growth by the extended finite element and level sets-Part I: Mechanical model. *International Journal for Numerical Methods in Engineering*, vol. 53, issue 11, pp. 2549-2568.

Murakami, K. (1987): *Stress Intensity Factors Handbook*. Pergamon Press, Oxford

Nishioka, T.; Atluri, S.N. (1982): Analytical solution for embedded elliptical cracks and finite element alternating method for elliptical surface cracks, subjected to arbitrary loadings. *Engineering Fracture Mechanics*, vol. 17, pp. 247-268.

Nishioka, T.; Atluri, S. N. (1983): Path-independent integrals, energy release rates, and general solutions of near-tip fields in mixed-mode dynamic fracture mechanics. *Engineering Fracture Mechanics*, vol. 18, issue 1, pp.1-22.

Nikishkov, G. P.; Atluri, S. N. (1987a): An equivalent domain integral method for

computing crack-tip integral parameters in non-elastic, thermo-mechanical fracture. Engineering Fracture Mechanics, vol. 26, issue 6, pp. 851-867.

Nikishkov, G.P.; Atluri, S.N. (1987b): Calculation of fracture mechanics parameters for an arbitrary three-dimensional crack by the equivalent domain integral method. *International Journal of Numerical Methods in Engineering*, vol. 24, pp. 851-867.

Nikishkov, G. P..; Park, J. H.; Atluri, S. N. (2001): SGBEM-FEM alternating method for analyzing 3D non-planar cracks and their growth in structural components. CMES: *Computer Modeling in Engineering & Sciences*, vol.2, no.3, pp.401-422.

Okada, H.; Rajiyah, H.; Atluri, S. N. (1988): A Novel Displacement Gradient Boundary Element Method for Elastic Stress Analysis with High Accuracy, *Journal of Applied Mechanics*, vol. 55, pp. 786-794.

Okada, H.; Rajiyah, H.; Atluri, S. N. (1989): Non-hyper-singular integral representations for velocity (displacement) gradients in elastic/plastic solids (small or finite deformations), *Computational Mechanics.*, vol. 4, no. 3, pp. 165-175.

O'Donoghue, P. E.; Atluri, S. N.; Pipkins, D. S. (1995): Computational strategies for fatigue crack growth in three dimensions with application to aircraft components. *Engineering fracture mechanics*, vol. 52, issue 1, pp. 51-64.

Park, J. H.; Ogiso, T.; Atluri, S. N. (1992): Analysis of cracks in aging aircraft structures, with and without composite-patch repairs. *Computational mechanics*, vol. 10, issue 3-4, pp. 169-201.

Park, J. H.; Singh, R.; Pyo, C. R.; Atluri, S. N. (1995): Integrity of aircraft structural elements with multi-site fatigue damage. *Engineering fracture mechanics*, vol. 51, issue 3, pp. 361-380.

Park, J. H.; Atluri, S. N. (1998): Mixed mode fatigue growth of curved cracks emanating from fastener holes in aircraft lap joints. *Computational Mechanics*, vol. 21, issue 6, pp. 1333-1336.

Pyo, C. R.; Okada, H.; Atluri, S. N. (1995): Residual strength prediction for aircraft panels with Multiple Site Damage, using the "EPFEAM" for stable crack growth analysis. *Computational mechanics*, vol. 16, issue 3, pp. 190-196.

Rice, J. R. (1968): A path independent integral and the approximate analysis of strain concentration by notches and cracks. ASME: *Journal of Applied Mechanics*, vol. 35, issue 2, pp. 379-386.

Rizzo, F. J. (1967). *An integral equation approach to boundary value problems of classical elastostatics. Quart. Appl. Math,* vol. 25, issue 1, pp. 83-95.

Special Issue: Extended Finite Element Method. *International Journal for Nu-*

merical Methods in Engineering, vol. 86, issue 4-5, page 403-666, 2011.

Stazi, F. L.; Budyn, E.; Chessa, J., Belytschko, T. (2003). An extended finite element method with higher-order elements for curved cracks. *Computational Mechanics*, vol. 31, issue 1-2, pp. 38-48.

Stolarska, M.; Chopp, D. L.; Moës, N.; Belytschko, T. (2001): Modeling crack growth by level sets in the extended finite element method. *International Journal for Numerical Methods in Engineering*, Vol. 51, issue 8, pp. 943-960.

Sukumar, N.; Chopp, D. L.; Moran, B. (2003): Extended finite element method and fast marching method for three-dimensional fatigue crack propagation. *Engineering Fracture Mechanics*, Vol. 70, issue 1, pp. 29-48.

Sukumar, N.; Chopp, D. L.; Béchet, E.; Moës, N. (2008). Three-dimensional non-planar crack growth by a coupled extended finite element and fast marching method. *International journal for numerical methods in engineering*, Vol. 76, issue 5, pp. 727-748.

Tada, H.; Paris; P. C.; Irwin, G. R. (2000): *The stress analysis of cracks handbook* (Vol. 130). New York: ASME press.

Tong, P; Pian T. H. H; Lasry S. J. (1973): A hybrid-element approach to crack problems in plane elasticity. *International Journal for Numerical Methods in Engineering, vol. 7, issue 3, pp. 297-308.*

Vijayakumar, K; Atluri, S. N. (1981): An embedded elliptical crack, in an infinite solid, subject to arbitrary crack-face tractions. *ASME, Journal of Applied Mechanics,* vol. 103, no. 1, pp. 88-96.

Williams, R. C.; Phan, A. V.; Tippur, H. V.; Kaplan, T.; Gray, L. J. (2007): SGBEM analysis of crack–particle(s) interactions due to elastic constants mismatch. *Engineering fracture mechanics*, vol. 74, no. 3, pp. 314-331.

XFEM 2009: *The Extended Finite Element Method – Recent Developments and Applications*. September 28 - 30, 2009, Aachen, Germany.

XFEM 2011: *The Extended Finite Element Method – Partition of Unity Enrichment: Recent Developments and Applications.* June 29 – July 1, 2011, Cardiff, UK.

XFEM 2013: *The Extended Finite Element Method – XFEM, GFEM, and Fictitious Domain Methods: Recent Developments and Applications*. September 11 - 13, 2013, Lyon, France.